SENSITIVITY OF OXYGEN MINIMUM ZONES DUE TO CARBON DIOXIDE RADIATIVE FORCING USING CESM 1.2

by

KRISTINA WOLFE

THESIS

Submitted in partial fulfillment of the requirements for the degree of Master of Science in Environmental Science at

The University of Texas at Arlington

May, 2019

Arlington, Texas

Supervising Committee:

Arne Winguth, Supervising Professor

Majie Fan

James Grover

Acknowledgements

I would like to thank my thesis advisor, Dr. Arne Winguth, of the Earth and Environmental Science Department at the University of Texas at Arlington. He was always available when I needed assistance or had a question about my research and, while allowing this paper to be my own work, guided me in the right direction whenever he thought I needed it. Taylor Huglett and Kelin Zhuang, postdoctoral researchers at the University of Texas at Arlington, were both of great help and assistance. I have Kelin Zhuang to thank for running the model simulations for this research. I would also like to acknowledge the high-performance computing support from Cheyenne, provided from the National Center for Atmospheric Research's (NCAR) Computational and Information Systems, which are sponsored by the National Science Foundation. All model simulations are carried out on the NCAR Wyoming Super Computing center, which is supported by the National Science Foundation (NSF).

Abstract

SENSITIVITY OF OXYGEN MINIMUM ZONES DUE TO CARBON DIOXIDE RADIATIVE FORCING USING CESM1.2

Kristina Wolfe, M.S.

The University of Texas at Arlington, 2019

Supervising Professor: Arne Winguth

Anthropogenic-induced climate change is occurring at an unprecedented rapid rate, compared to the geologic past. In this study, CO_2 stabilization scenarios (1x, 2x, and 4x preindustrial atmospheric pCO_2 levels) utilizing the Community Earth System Model (CESM) are carried out to assess the response of oxygen minimum zones to net primary production and vertical carbon fluxes in a changing climate. Compared to the 1x CO_2 experiment, sea surface temperature (SST) rise in the 4x CO_2 scenario, to 3 °C to 5 °C in the Pacific and Atlantic Ocean, between 30 °S and 60 °S. In contrast, the North Atlantic Ocean and around Greenland cools by 6.5 °C which is linked to the weakening of the Atlantic meridional overturning circulation (AMOC). In the 4x scenario, export production decreases in the northern Atlantic Ocean, consistent to the cooling and reduced AMOC, and in the central equatorial Atlantic and Pacific Ocean, due to reduced Ekman-induced upwelling and associated decline in surface nutrient concentration. In contrast, export production increases in the region of the Antarctic Circumpolar Current (ACC), linked to a rise in surface phosphate (PO_4) concentration. Surface nitrates (NO_3) decrease globally, especially around the equator. Dissolved Oxygen (DO) concentration at intermediate depth of equatorial Atlantic and Pacific Ocean water masses decreases from 1x CO_2 to the 4x CO_2,

linked to both a decrease in Apparent Oxygen Utilization (AOU) and decline in oxygen solubility by the warming.

Table of Contents

List of Illustrations

Chapter One: Introduction

Since the industrial revolution, anthropogenic-induced rise in greenhouse gases by emission from fossil fuel and land use changes, and associated climate change, has been occurring and rapidly growing at a near-exponential rate when compared to the geological past. The most abundantly emitted greenhouse gas is carbon dioxide (CO_2) which has increased from 278 ppmv in 1740 (Fig. 1) (Keeling et al., 2001) to 411 ppmv in 2019 (NOAA, 2019). Approximately 40% of these anthropogenic-induced carbon emissions have remained in the atmosphere, whereas the carbon uptake by land and ocean is ~30% each (IPCC, 2013). Increase in CO_2 accumulation in the atmosphere by reduced uptake in the ocean and reduced solubility and circulation have caused a positive climate-carbon cycle feedback that further enhanced the warming (Cox et al., 2000; Dufresne et al, 2002).

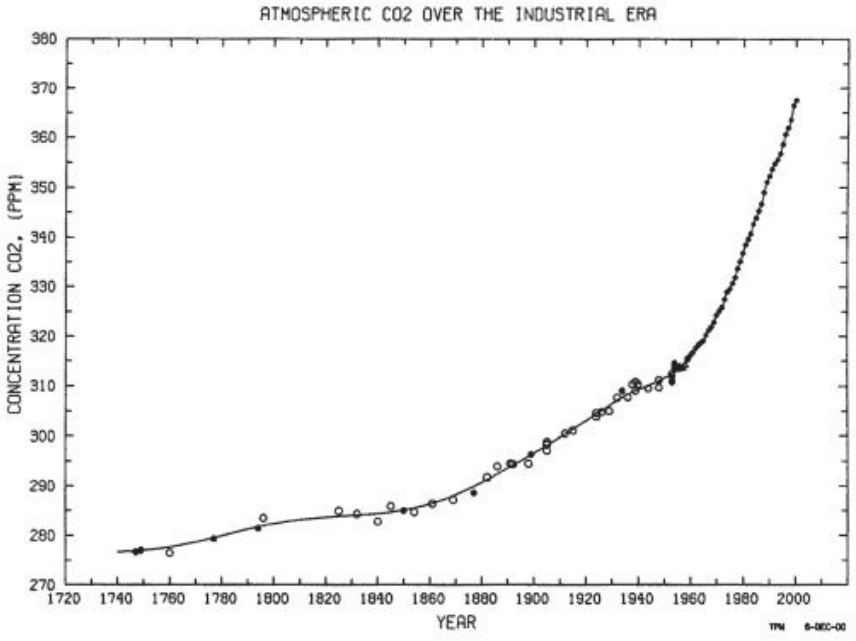

Figure 1. Global averages of greenhouse gases have increased for CO_2 (Keeling et al., 2001).

Rising sea temperatures, in response to CO_2-radiative forcing, and the subsequent decrease in upwelling and increase in upper ocean stratification, affect biogeochemical cycles such as deoxygenation across all time scales. The air-sea gas exchange of oxygen between atmosphere and the ocean depends on wind speed and temperature (Wanninkhof, 1992). With rising sea temperatures from anthropogenic climate change, sea surface concentrations of O_2 will be depleted due to reduced solubility. O_2 gas (g) in solution depends on solubility and [O_2] following the Henry Law:

$$O_2(g) = \frac{[O_2]}{K_0} \quad (1)$$

K_0 is the temperature and salinity dependent solubility coefficient of dissolved O_2 concentration (DO) in seawater (Weiss, 1970). The vertical dissolved oxygen distribution in the sea is controlled by physical and biological processes (solubility and biological pumps respectively; Volk and Hoffert, 1985) and DO is produced at the surface by photosynthesis using the following equation:

$$6CO_2 + 6H_2O \leftrightarrow C_6H_{12}O_6 + 6O_2 \quad (2)$$

Advection and mixing affect the DO concentration in the ocean as well (Keeling and Garcia, 2002), however, an increase in stratification will reduce primary production, and thus the particulate organic carbon flux, which can lead to an increase the DO concentration in the interior ocean.

Most of the elements, like carbon, phosphate, and nitrogen (Fig. 2) will be recycled in the ocean. Nitrogen is absorbed into the ocean as N_2 through the air-sea gas exchange. Phytoplankton then assimilate nitrogen in the euphotic zone. Ammonification is caused by bacteria, which is responsible for denitrification in the euphotic zone. Phosphorous is also

assimilated and consumed by phytoplankton. Dissolved phosphorous is then incorporated in the organic remains and precipitated to the bottom of the sea, some of which gets buried in the sediment, causing an increase in atmospheric O_2 (Fig. 3), but only a small fraction equivalent to riverine input is buried in the ocean sediments (Archer, 2003). Carbon (C), hydrogen (H), nitrogen (N), oxygen (O), and phosphorus (P) ratio in marine organic matter are in approximate stoichiometric ratios (Redfield, 1934), with the ratio of C: N: P being the mole ratio of 106:16:1. A large portion of organic matter is remineralized, leading to a decline in dissolved oxygen below the euphotic zone (eq. 2).

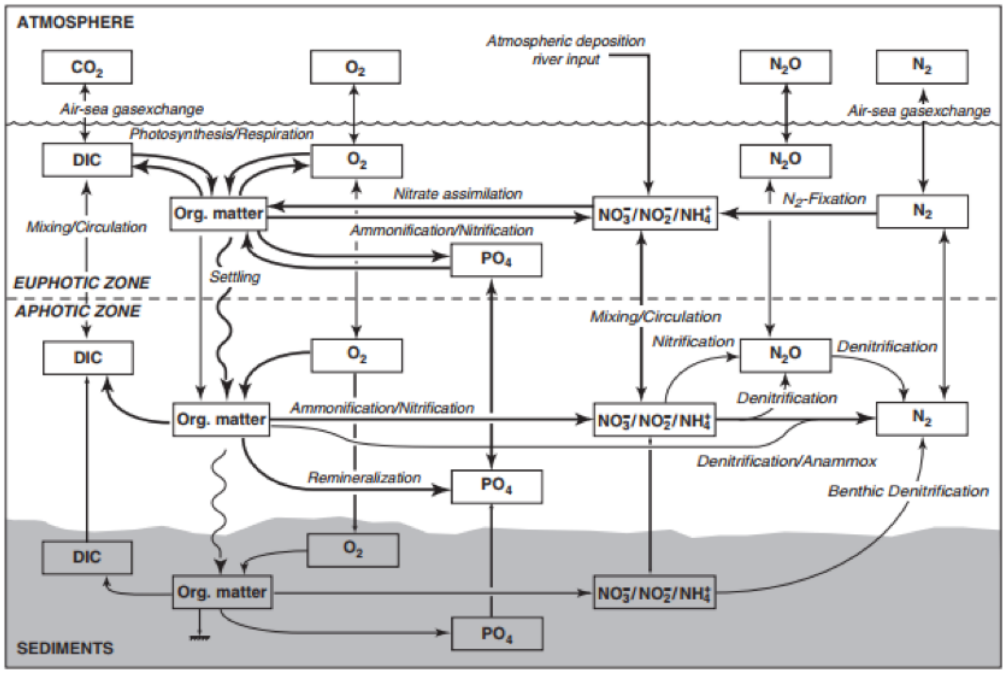

Figure 2. Presented is a Schematic representation of the marine nitrogen cycle and its coupling to the marine cycles of oxygen, phosphorus, and carbon (Gruber, 2008).

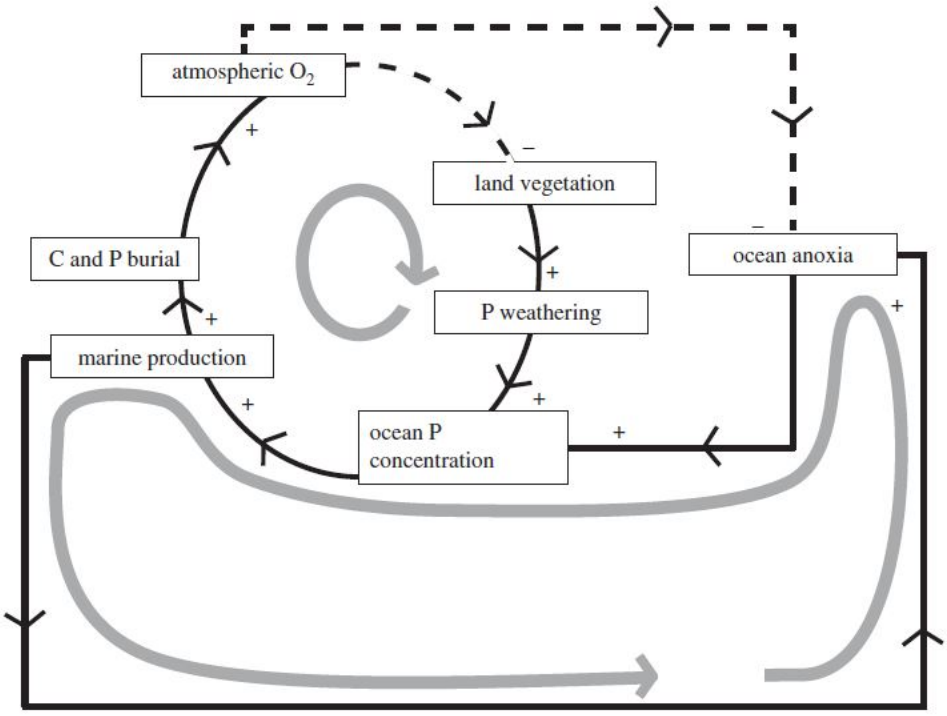

Figure 3. Earth system interactions are linked for atmospheric oxygen and ocean nutrients. The direct relations are represented by solid lines with a plus sign and the inverse relations are shown by a dashed line with a minus sign. Arrows describing a closed circuit indicate a negative feedback loop and either a positive feedback or loop or no feedback loop is indicated where there is one dashed arrow in the loop. The upper thick grey line is a negative feedback loop and the lower loop is a positive feedback loop (Watson et al., 2017).

Obligate aerobes rely upon DO to produce adenosine triphosphate (ATP), thus a decrease in its concentration could negatively impact the ocean's net primary production (NPP) and reduce the biological pump. DO concentrations below 60 µM is hypoxic, which is lethal for more than 50% of marine benthic organisms, and DO < 20 µM can kill higher trophic level organisms (e.g. fish). DO concentrations below 10 µM is lethal for more than 90% of marine species. When DO concentrations are < 5 µM, nitrogen is removed dominantly by denitrification and anaerobic ammonium oxidation (Deutsch et al., 2011) and when it is < 1 µM, only specifically adapted microbes can exist. At severe hypoxia, microbes convert nitrite and ammonium to nitrogen gas which removes nitrogen from the water and limits primary production (Karstensen et al., 2015).

A reduction of biotic life in the ocean could potentially reduce vital nutrients such as NO_3 and PO_4.

Oxygen minimum zones (OMZ) typically develop beneath upwelling regions linked to high particulate organic carbon (POC) flux. The decay of POC together with advection of DO determine the extent of the OMZs (Cabre et al., 2015). Two of the largest OMZs are in the east tropical Pacific, north and south of the equator. Low Oxygen Zones (LOZ) occur also in the tropical North Atlantic Ocean. These zones are created beneath the mixed layer, the euphotic zone, and modewater eddies. Note that the DO concentration is typically lowest in the center of eddies with net respiration rates of 3 to 5 times higher in adjacent water masses. Diurnal vertical migration of zooplankton is suppressed in eddies, a direct impact of open dead zones on the marine ecosystem (Karstensen et al., 2015).

An increase of dissolved CO_2 levels in the ocean will lead to higher ocean acidity that can dissolve calcareous shells, weakening the vertical carbon flux and thus the biological pump (e.g. Heinze et al., 2004). Increase in ocean acidification results from anthropogenic CO_2 invasion into the ocean can affect thus the DO distribution in the ocean, the concentration of which is balanced between oxygen production (photosynthesis), consumption (respiration and other chemical reactions), and exchange with the atmosphere. Ocean acidification will also reduce the ocean's uptake capacity for anthropogenic CO_2 and could change the carbon-to-nitrogen stoichiometric rations of marine phytoplankton, which may show an increase for photosynthesis due to the availability of dissolved CO_2, causing significant changes to the marine distribution of oxygen due to its effect on oxygen demand during remineralization of organic matter (Gruber, 2011).

With an increase in CO_2 radiative forcing rise in ocean temperatures, there will be an increase in stratification, solubility, and concentration of CO_2 as DO decreases (Cabre et al., 2015, Ito and Deutsch, 2010; IPCC, 2013). By the end of this century, it has been predicted that DO will decline 4 – 7% (Matear, 2003). An apparent oxygen decline was documented in the subtropical modewater of the North Atlantic at the Bermuda Atlantic Time Series site from the 1980s to 2000s (Stanley et al, 2012) and a decrease of O_2 and increase of apparent oxygen utilization (AOU) was simulated in the upper ocean isopyncnals using CESM Large Ensemble (Long et al., 2016). Increase of export production stimulated by the warming will increase remineralization of the sinking particulate organic carbon (POC), causing rapid depletion of subsurface oxygen and reducing interior oxygen concentration. A decreased ventilation rate increases residence time of subsurface waters, which allows more particulate organic matter (POM) remineralization to occur, further reducing oxygen concentration in the ocean (Fig. 4). Currently, the lowest oxygen concentrations are found in the thermocline (Matear, 2003). Changes in oxygen can be caused by changes in AOU or Oxygen Saturation (O_2sat) with the equation:

$$\Delta O_2 = O_2 sat - \Delta AOU \quad (3)$$

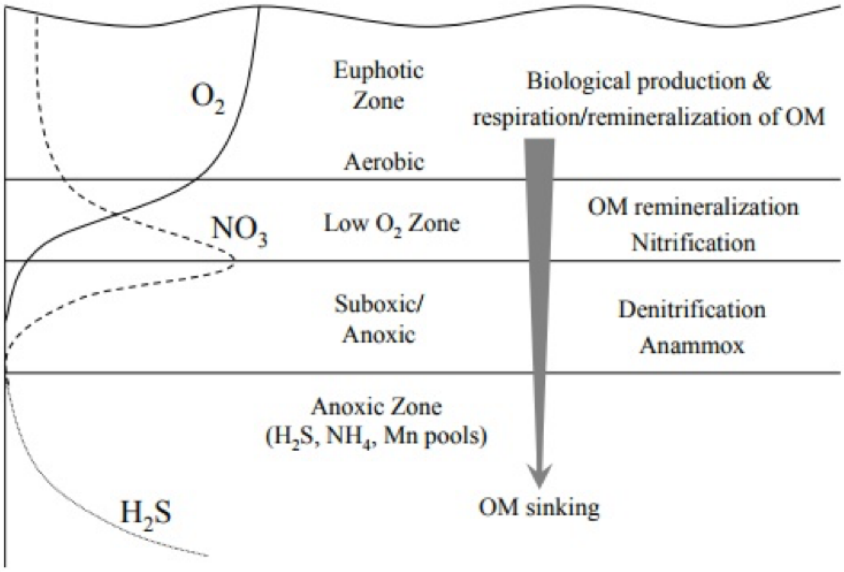

Figure 4. A schematic vertical profile of water column process shows the well oxygenated euphotic zone, oxycline/upper nitricline region, suboxic zone, and anoxic zone. POM = particulate organic matter (Pena et al., 2010).

Shifts in ecosystems, as well as mass extinctions, have occurred during periods when the oxygen content in the ocean was low. Atmospheric oxygen concentrations increased around 2.4 billion years ago due to the evolution of life (Knoll and Carroll, 1999) and then low atmospheric concentrations of oxygen 542 million years ago, during the Phanerozoic, led together with oceanic hypoxia and numerous anoxic events to mass extinctions. Biotic life declined 385-360 million years ago, during the Devonian and Carboniferous periods, when shallow continental seas suffered wide-spread anoxia. The Permian-Triassic extinction that occurred 252 million years ago brought about a 90% loss of all marine animal life when both shallow marine and deep ocean environments were widely anoxic (Erwin, 2006). According to the historical record, the extent of oxygen-depleted waters and OMZs are sensitive to climate and many anoxic events in the ocean have coincided with times of elevated atmospheric carbon dioxide (Falkowski et al., 2011), making current and future anthropogenic climate change due to an increase of anthropogenic

CO_2 of concern to marine life because of widespread mortality and extended areas of hypoxic or anoxic conditions (Stramma et al., 2012).

Chapter Two: Objective

This study focuses on the decline in DO concentration and the extent of the OMZs in response to climate-induced changes in solubility, NPP, and vertical carbon fluxes linked to an increase in CO_2 radiative forcing. For this purpose, a set of simulations with a Community Earth System Model (CESM) are analyzed. A preindustrial reference simulation is compared with two CO_2 radiative forcing sensitivity experiments, one with 2x and the other with 4x the preindustrial atmospheric CO_2 level. The goal is to predict changes in OMZ extent and understand biogeochemical and physical processes that contribute to these changes.

Chapter Three: Model Description

In this study, a fully-coupled general atmosphere-ocean circulation and biogeochemical cycling model of the ~1° x 1° horizontally resolved CESM 1.2.2 (Hurrell et al., 2013), is used. It has interactive carbon-nitrogen cycling, a marine ecosystem-biogeochemical model, and new chemical and physical processes to study aerosol effects on climate and consists of the Community Atmospheric General Circulation Model version 4 (CAM4), the Parallel Ocean Program version 2 (POP2), a general model of the ocean circulation, a dynamic sea ice model, the Community Ice Code version 4 (CICE4), and a Community Land Model version 4 (CLM4) (Gent et al., 2011).

Several improvements have been made to CAM4 from the previous version. CAM4 has an improved representation of deep convection that occurs less frequently in comparison to CAM3. CAM4 uses a horizontal grid for latitude/longitude with 280 x 200 points, giving a uniform resolution of 1˚ version and half the number of grid points in the 2˚ version. CAM4 uses 26 layers in the vertical (Gent et al., 2011).

POP2 utilize a nominal Gaussian ~1˚ grid. In the Northern Hemisphere, the pole is displaced over Greenland whereas in the Southern Hemisphere over Antarctica. Resolution is uniformly 1.11˚ in the zonal direction and the horizontal grid has 320 x 384 points. The meridional resolution gradually increases from 0.27˚ around the equator, to 0.54˚N and 0.54˚S and it is constant at higher latitudes (Gent et al., 2011). There are 60 vertical levels at depths from 10 m in the top 150 m and increase to 250 m below 4000 m (Hurrell et al., 2013).

Biogeochemical Elemental Cycling (BEC) model simulates ocean biogeochemistry and lower-trophic-level marine ecosystem dynamics. This ecosystem model is adapted from Doney et al. (1996) and includes several phytoplankton functional groups, such as diatoms, diazotrophs, cocolithiphores, and a smaller phytoplankton. (Moore et al., 2002, Moore et al., 2004, Moore et al, 2013). The growth rates of phytoplankton are determined by light and nutrient availability and use a modified form of a growth model by Geider et al. (1998) and phosphorus and nitrogen maximum and minimum values from Geider et al. (1998) are used. The BEC model uses these groups to track the cycling of carbon, nitrogen, phosphorous, iron, silicon, and oxygen (Moore et al., 2013).

The biogeochemical model is coupled to an ocean biogeochemical model that affects the physical climate by providing the surface chlorophyll concentrations that depends on the absorption profile of shortwave radiation in the ocean. This model also considers air-sea gas exchange with atmospheric pCO_2. In addition, it has an atmospheric chemistry package and an enhanced atmospheric physics parameterizations. The atmospheric model uses prescribed anthropogenic CO_2 surface fluxes from fossil fuel emissions and land use changes. The sum of the surface fluxes is used as a surface boundary condition. These fluxes are the atmospheric tracer for the ocean, land, and fossil fuel fluxes and one net CO_2 tracer. The atmospheric model then transports the tracers as dry mixing rations. The column average of the net CO_2 tracer is used in atmospheric radiative transfer computations and the net CO_2 tracer in the bottom layer is used in terrestrial photosynthesis and sea-to-air-flux computations (Lindsay et al., 2014).

CLM4 has many additional capabilities, input datasets, and updates to the parameterization. A carbon-nitrogen (CN) cycle component is included that is prognostic in

carbon and nitrogen, though the fluxes for carbon and nitrogen are diagnostic and not passed to the atmosphere. The CN component impacts climate through season and interannual vegetation phenology. River discharge has been separated into streams of liquid and water and the global heat conservation has been improved since heat from the ocean component is needed to melt the ice (Gent et al., 2011).

Important developments have been added to CICE4. A new radiative transfer scheme was incorporated. Inherent optical properties defining scattering and absorption characteristics of snow, sea ice, and absorbers are used by the delta-Eddington radiative transfer which allows for melt pond and absorbers to be incorporated. Much more realistic surface ice albedos are also used in this version than in CCSM3. The horizontal grid for the ocean component is used for the sea ice component (Gent et al., 2011).

For the preindustrial control run, the year 1850 was used because the CO_2 and aerosol concentrations were closer to the preindustrial levels in 1850. The 1x CO_2 scenario was initialized from a 1000-year simulation and then integrated for 150 years to reach a quasi-steady state for the upper ocean. Additional runs were made for 2x CO_2 and 4x CO_2 and the annual average of the last ten model years of each run (1x CO_2, 2x CO_2, and 4x CO_2) were analyzed for the effect upon oxygen, nutrients, and NPP.

Chapter Four: Results

The difference of SST between the 2x CO_2 and 1x CO_2 experiment is displayed in (Fig. 5). The 4x CO_2 scenario, when compared to the 1x CO_2 experiment, a rise in SST of 3 °C to 5 °C, in Pacific and Atlantic Ocean, between 30 °S and 60 °S. A cooling anomaly of 6.5 C occurs in the North Atlantic Ocean, between 30°N and 60°N, because of reduced poleward heat transport. This pattern is intensified in the 4x CO_2 scenario relative to the 1x CO_2 experiment. Compared to the 1x CO_2 scenario, the SST rises globally, with the greatest change of 2°C -6°C in the Southern Ocean, whereas the cooling anomaly in the North Atlantic Ocean is increased compared to the difference between the 2x CO_2 and 1x CO_2 experiment. This cooling is in line with the observed cooling trend in the North Atlantic Ocean since the mid-2000s (Schmidtko et al., 2017), which has been linked to the variability in the Gulf Stream-Subpolar Gyre system and associated weakening of deep water formation and Atlantic Meridional Overturning Circulation (AMOC) (Manabe et al., 1991, Manabe and Stouffer, 1993). From 1995-2005, density anomalies became negative during a pronounced warming of the subpolar gyre, which decreased the strength of the formation of North Atlantic deep waters (NADW). This led to a cooling from a negative anomaly in the meridional heat transport. A positive temperature anomaly in the northern subpolar region occurs between the 4x CO_2 and 1x CO_2 scenario, due to the cooling of the region along the path of the Gulf Stream (Ruiz-Barradas et al., 2018). Large-scale changes occurring in ocean circulation can have a significant effect on surface temperature and these changes in surface temperature cannot be neglected because they are crucial for the behavior of the thermohaline circulation (Rahmstorf and Willenbrand, 1995).

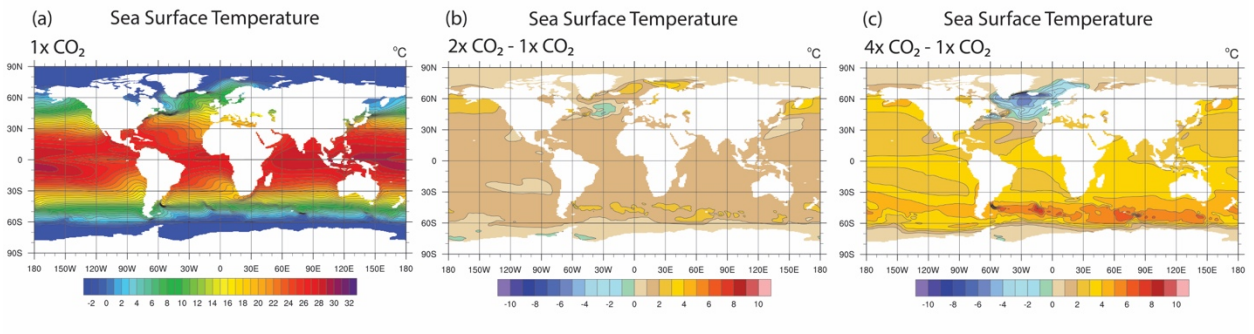

Figure 5. Sea surface temperature (SST) simulated by CESM1.2 for 1x CO_2 (a), 2x CO_2 minus 1x CO_2 experiment (b), and 4x CO_2 minus 1x CO_2 experiment (c).

Potential temperature is the temperature a water mass would have if it were moved adiabatically. The SST differences between 2x CO_2 and 1 x CO_2 scenario for the upper 2000 m of the Atlantic Ocean, along 20°W, reveal an ocean warming with CO_2 radiative forcing (Fig. 6). A cooling anomaly in the North Atlantic is noticeable between 30°N-60°N, in the upper 1000 m. Potential temperature is increasing slightly between 30°S-60°S. This difference in the upper 2000 m increased considerably in when compared the 4x CO_2 scenario with 1x CO_2 scenario. Potential temperature difference is higher in the upper 2000 m along the equator and tropical regions, likely in response to an increase of surface air temperature and thermal stratification.

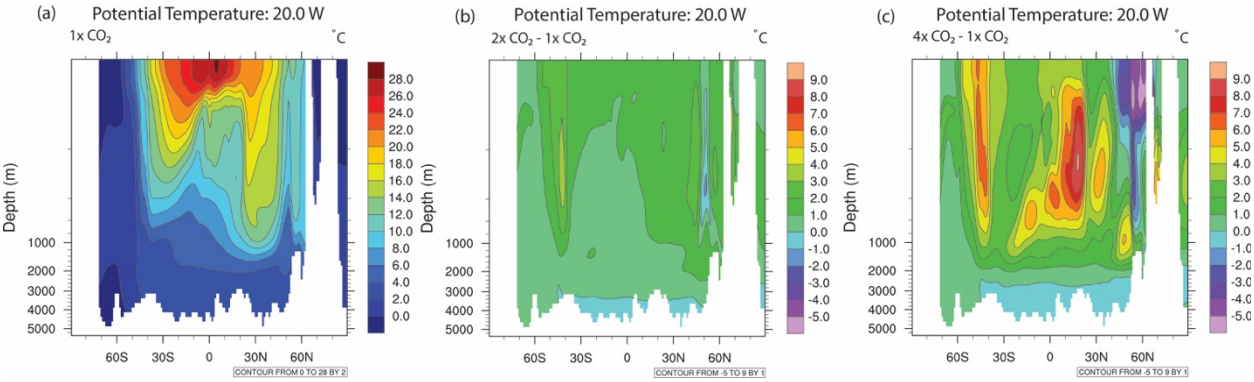

Figure 6. Cross section of potential temperature at 20.0°W simulated by CESM1.2 for 1x CO_2 experiment(a), 2x CO_2 – 1x CO_2 experiment (b) and 4x CO_2 -1x CO_2 experiment (c).

Ekman-induced upwelling and downwelling is of importance for the biogeochemical tracers in the ocean. Intense Ekman-upwelling occur along the equatorial divergence in the 1x CO_2 scenario (Fig. 7). In the center of subtropical gyres, Ekman-induced convergence lead to downwelling. Ekman-induced upwelling occurs along the west coasts of the continents from shallow depth <300 m. The upwelled water masses have nutrient concentration, thus promoting primary productivity. As part of the Stommel and Arons's (1960) abysall upwelling from nutrient-rich layers of the deep ocean with the upper layer of ocean transporting nutrients to the surface (Velez-Belchi and Tintore, 2001).

In the 2x and 4x CO_2 scenarios, upwelling is decreasing in coastal and equatorial upwelling areas. There is a weak permanent annual upwelling zone at 26-35 °N, a permanent annual upwelling zone at 21-26 °N, the Mauritania-Senegalese upwelling zone at 12-19 °N, and the canary upwelling ecosystem (CUE) off northwest Africa at 11-35 °N. Note that persistent winds are needed in order for Ekman-induced upwelling to occur along the west coasts (e.g. Cropper et al., 2014). This decrease in coastal upwelling could be due to decline in the strength of trade winds (e.g. Hsieh and Boer, 1992).

In the Southern Ocean, however, upwelling is intensified in global warming scenarios. Upwelling is increasing in the subtropical Atlantic Ocean, around 23.5 °S and in the Southern Ocean, south of 60 °S, for both the 2x CO_2 and the 4x CO_2 scenarios. Increase wind stress in the Southern Ocean in these scenarios are linked with a stronger polar vortex compared to the 1x CO_2 scenarios and this rise in wind stress could amplify convective overturning. This convection could mix nutrients to the surface and thus stimulate primary productivity (Lauderdale et al., 2013).

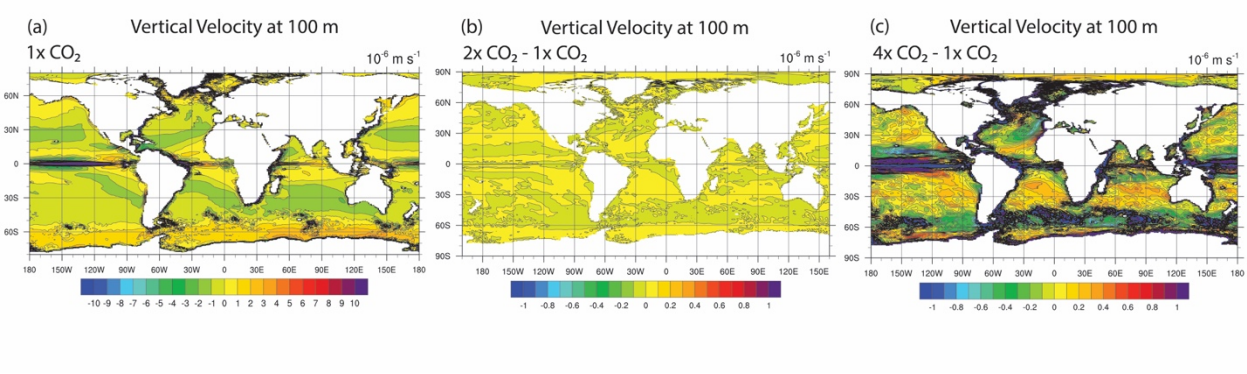

Figure 7. Vertical velocity simulated with CESM1.2 at 100 m for 1x CO_2 (a), the difference between 2x CO_2 minus 1x CO_2 experiment (b), and 4x CO_2 minus 1x CO_2 experiment (c).

The surface mixed layer in the ocean is where salinity, temperature, and density are vertically uniform due to wind-induced turbulent mixing. The mixed layer thickness influences the heat content of the ocean. It is important to analyze the mixed layer depth, in the context of analyzing oxygen minimum zone, and its effect on biological activity, however, the oxygen estimate in model validations may be biased in regions of Ekman pumping or strong biological activity (de Boyer Montegut et al., 2004).

With the increase of SST due to anthropogenic climate change, upper ocean stratification is expected and most of the heat is being absorbed near the surface of the ocean, whereas deep ocean changes have been minimal. Surface warming enhances the vertical surface density gradient and thus ocean stratification. Though surface warming stimulates productivity, stratification and reduced nutrient supply reduce marine productivity. Ocean stratification can be diminished by wind-driven divergence (Somavilla et al., 2017) but increased stratification in the upper ocean could counteract the effects of Ekman-induced upwelling (Bakun et al., 2015).

In the 1x CO_2 scenario (Fig. 8), the mixed layer depth is deepest in the temperate latitudes of the Atlantic Ocean, particularly in the North Atlantic Ocean linked to winter cooling. When anthropogenic CO_2 is doubled, the mixed layer gets shallower throughout most of the ocean, but not uniformly. The most notable change is an increase in the depth of the mixed layer in the North Atlantic Ocean, due to reduced temperature contrast between land and ocean. In the Southern Ocean however, the mixed layer deepens with CO_2 radiative forcing due to surface cooling and increased wind stress. Similar changes occur when CO_2 concentration in the atmosphere is quadrupled. Note, that the Northern North Atlantic stability is lower in the 4x CO_2 scenario compared to the 1x CO_2 because of retreat of sea ice (Manabe et al., 1991) and thus exposure of surface to cool air temperature advection from Greenland. Correspondingly, reduced sea ice cover in the Southern Ocean lead to deepening of the maximum mixed layer depth due to cold air advection in the 4x CO_2 scenario compared to the 1x CO_2 experiment.

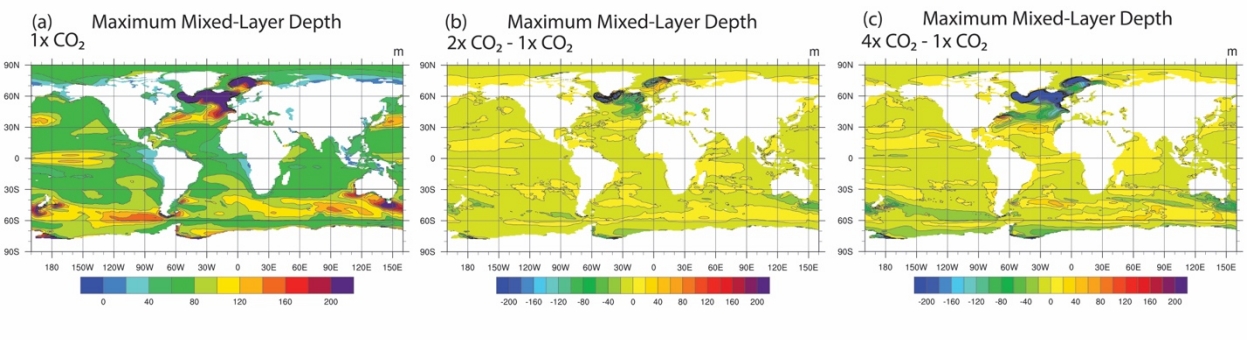

Figure 8. Maximum Mixed-Layer Depth simulated by CESM1.2 for 1x CO_2 experiment (a), and the difference between 2x CO_2 minus 1x CO_2 experiment (b) and 4x CO_2 minus 1x CO_2 experiment (c).

The North Atlantic meridional overturning occurs predominately during the wintertime due to heat release from water masses that originated from the North Atlantic Current. Previous model studies, when calibrated with SST data, estimated that the Atlantic meridonal overturning circulation (AMOC) has declined in strength by 15% since the industrial era, probaly due to global warming caused by anthropogenic climate greenhouse gas emissions, which may have added fresh water to the surface ocean from the melting of the Greenland Icesheet, and this would have led to a reduction in density of the North Atlantic Ocean water (Cesar et al., 2018; Praetorius, 2018).

When atmospheric CO_2 is doubled (Fig. 9), a decrease of approximately 10 Sverdrups (Sv) is simulated in the North Atlantic Ocean. A quadrupling of atmospheric CO_2 leads to a much greater decrease and slowdown in the AMOC, by approximately 20 Sv, compared to the 2x CO_2 experiment. The largest decrease is still in the temperate latitudes of the North Atlantic Ocean, but the range of the decrease is becoming more pronounced throughout the Atlantic Ocean. A freshening of the North Atlantic Ocean, due to enhanced precipitation and increased SST, could be responsible for the decline in the simulated AMOC with increase in CO_2 radiative forcing.

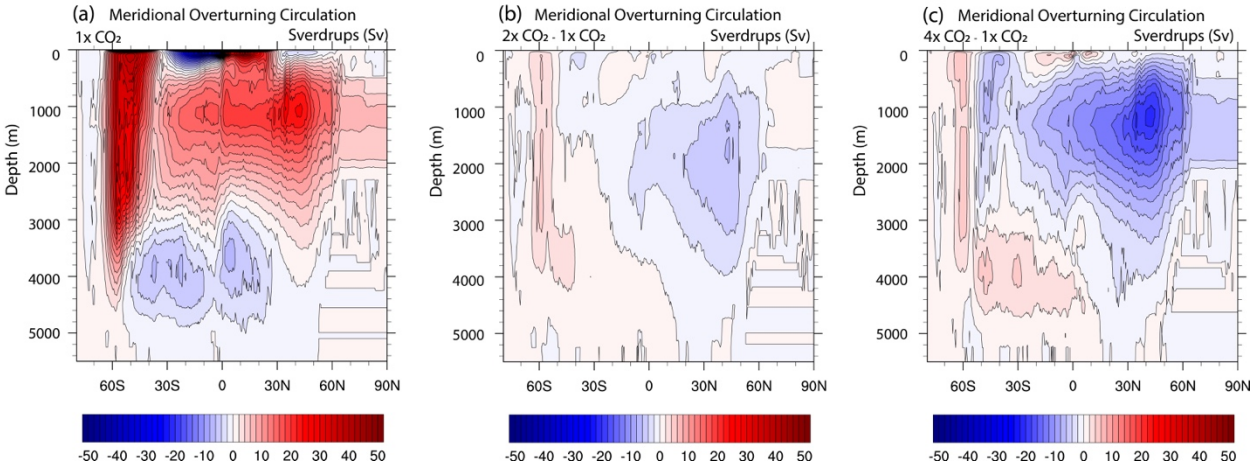

Figure 9. Atlantic Meridional Overturning Circulation is simulated by CESM1.2 for 1x CO_2 experiment (a), the difference of the 2x CO_2 minus the 1x CO_2 experiment (b), and the 4x CO_2 minus the 1x CO_2 experiment (c).

Idealized age is the average time it has taken for a particular water mass to make contact with the surface and be ventilated (Thiele and Sarmiento, 1990; England, 1995; Bryan et al., 2006). It is important to analyze the idealized age because this can impact important cycles, such as the distribution of tracer dissolved oxygen in the ocean (Gnanadesikan et al. 2007). Global warming is expected to increase ocean stratification (Gruber, 2011) and with increasing stratification, it can be expected that there would be less effective mixing and an older ocean interior (Gnanadesikan et al., 2007).

Idealized age was simulated at a depth of 1000 m for all three scenarios (Fig. 10). An increase in CO_2 radiative forcing resulted in the general decline in the ventilation of the abyss. Along the tropics, off the east coast of South America, the idealized age of Antarctic intermediate water at 1000 m is higher in the 2x CO_2 and 4x CO_2 scenarios compared to 1x scenario because of a reduction in the formation of Antarctic intermediate water masses, possibly due to an

increase of precipitation from the hydrological cycle and increase stratification near the subpolar front where the water mass forms (Sarmiento et al., 2004). Furthermore, a younger idealized age in regions with low DO results from increased mixing (Gnanadesikan et al., 2007). In the Southern Ocean, mid-latitude westerlies are simulated under global warming scenarios, and thus Ekman layer deepen in these scenarios. However, below this layer, the idealized age of the Southern Ocean is increasing in the 4x CO_2 scenario because of increased stratification.

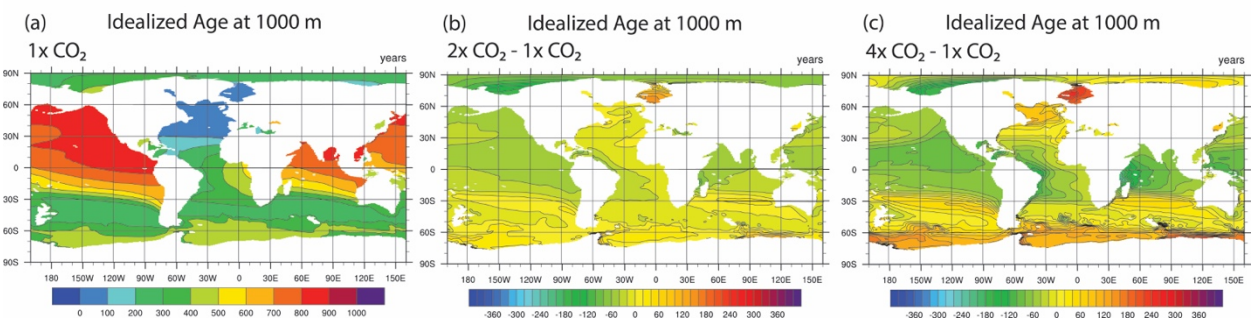

Figure 10. Idealized age simulated by CESM1.2 at 1000 m for a 1x CO_2 (a), the difference between 2x CO_2 and 1x CO_2 experiment (b) and the difference between 4x CO_2 and 1x CO_2 experiment (c).

In this model, the photosynthetic carbon fixation rate, minus the fraction of fixed carbon that is used for autotrophic planktonic microbes and benthic plants, is called Net Primary Production (NPP). This process can be influenced by atmospheric and oceanic processes, such as sea ice extent, currents, stratification, and upwelling. This model includes limiting nutrients, such as nitrogen, phosphorus, iron, and silicon, as we as light levels that regulate phytoplankton growth rates for key phytoplankton functional groups, such as diatoms and diazotrophs, which are modelled after *Trichodesmium* spp., and cocolithophores (Moore et al., 2002), and tracks the cycling of carbon, nitrogen, phosphorus, iron, silicon and oxygen, key elements in the ocean

(Moore et al., 2013). Basin-scale patterns of primary and export production are reproduced in the BEC model used in CESM (Moore at al., 2004). Anthropogenic climate change is expected to decrease NPP in the open ocean, although a slight increase is projected to occur at high latitudes (Boyd et al., 2014).

At 100 m, the base of the euphotic zone, the majority of NPP occurs along the tropics and in the Southern Ocean (Fig. 11). A decrease in NPP with an increase in CO_2 radiative forcing occurs in the North Atlantic Ocean, consistent with the cooling and reduced AMOC, and in the central equatorial Atlantic and Pacific Ocean, due to reduced Ekman-induced upwelling, and along the Southern Ocean. In the 4x CO_2 scenario, NPP in the Southern Ocean is lower compared to the 1x CO_2 scenario because of a decrease in the mixed layer depth and mixing (Fig. 6c, 7c, and 8c) (Gruber, 2011). Reduced NPP then leads to a reduction in POC which will increase DO. In the central North Atlantic Ocean, in the region of the Atlantic Circumpolar Current (ACC), NPP is higher in the 4x CO_2 than in the 1x CO_2 scenario. Cooler temperatures are observed in the North Atlantic Ocean under increased levels of CO_2 levels, which may be caused by the slowing down of the AMOC (Praetorius, 2018). Loss of sea ice from a rise in ocean temperatures could cause the ice edge to recede and erode stratification, providing increased light and access to nutrients, thereby enhancing NPP (Randelhoff and Sundfjord, 2018).

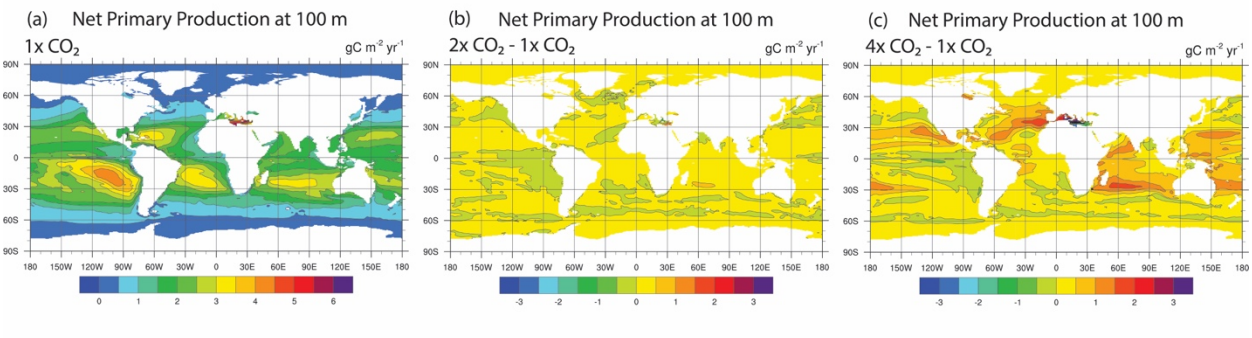

Figure 11. Net Primary Production (NPP) is simulated by CESM1.2 at 100 m for the 1x CO_2 experiment (a), difference between the 2xCO_2 scenario minus the 1xCO_2 scenario (b), and difference between the 4xCO_2 scenario minus the 1xCO_2 scenario (c).

Nitrate is one of the limiting nutrients for photosynthesis in the ocean. The concentration of nitrate follows the ocean circulation and biological pump (Smith et al., 2009). The size of the nitrogen reservoir can impact atmospheric CO_2 by limiting the effeciancy of the biological pump (Falkowski, 1997). Nitrate sources in the ocean are created by nitrogen fixation by cyanobacteria and riverine runoff whereas loss of nitrate occurs by sedimentation and in hypoxic zones by denitrification. In oxygen minimum zones, nitrate is consumed because under hypoxic conditions, aerobic bacteria may utilize the chemical binded oxygen during remineralization (Gnanadesikan et al., 2007).

The highest levels of inorganic nitrate in the Atlantic Ocean are within the upper 100 m in the Ekman-induced upwelling zones in the tropics and in the Southern Ocean where a significant amount of upwelling occurs (Fig. 12). Nitrate levels decrease globally along the surface of the ocean and from within the upper 1000 m of the Southern Ocean and equatorial region. In the 4x CO_2 scenario, reduced mixing in the North Atlantic lead to increased depletion of nutrients in the upper 200 m. Below this level, nutrient concentrations are increasing, which is linked to remineralization of particulate organic phosphorus (POP) and reduced ventilation.

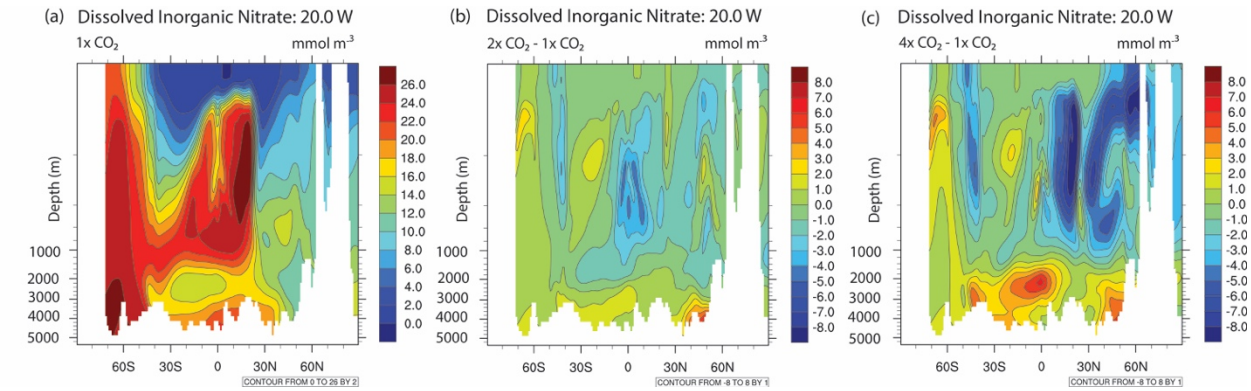

Figure 12. Section of dissolved inorganic nitrate (NO_3) in the Atlantic Ocean simulated by CESM1.2 for 1x CO_2 experiment (a) , differences between the 2x CO_2 experiment and 1x CO_2 experiment (b), and differences between the 4x CO_2 experiment and 1x CO_2 experiment (c).

In additon to nitrate, phosphorus is an important nutrient for phytoplankton growth. The upper water column of the Atlantic oceans is rich in nitrogen, carbon, and phosphorous. The majority of phosphorus in the ocean is recycled within the ocean with river-run-off input balanced by loss by sedimentation. Increased supply of phosphorous to the ocean lead to a higher ocean productivity and oxygen demand (Watson et al., 2017), but this effect is not simulated in this study. With an increase in CO_2 radiative forcing, phosphate concentration declines, similarly to the decline in nitrate concentration, within the upper 1000 m along the equatorial Atlantic

(Fig. 13). However, in the highly productive Southern Ocean, along the Antarctic circumpolar current (ACC), an increase in the phosphate concentration with CO_2 radiative forcing is predicted. With increasing temperature and a limit in nutrients, oxygen demand decreases in the subsurface.

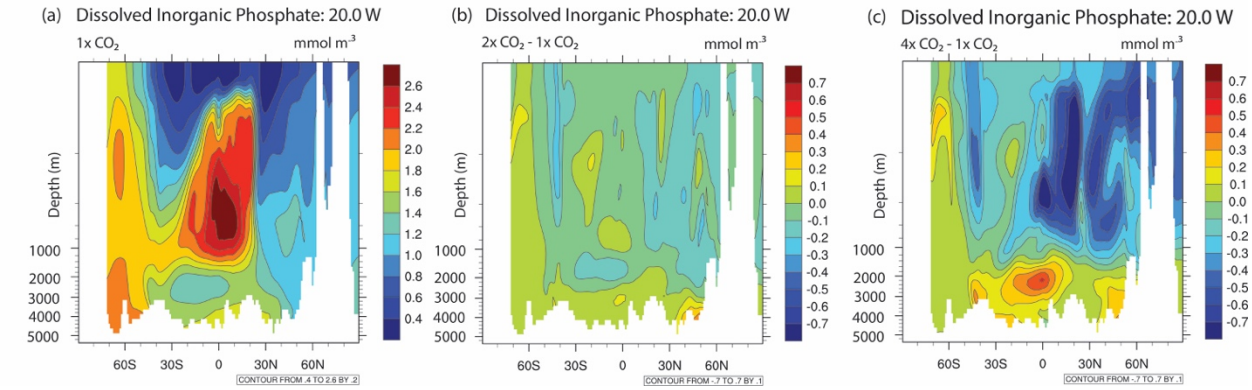

Figure 13. Cross-section of dissolved inorganic phosphate (PO_4) in the Atlantic Ocean simulated with CESM1.2 for 1x CO_2 experiment (a), differences between the 2x CO_2 experiment and 1x CO_2 experiment (b), and differences between the 4x CO_2 experiment and 1x CO_2 experiment (c).

The requirements of marine life for phosphorous, nitrogen and oxygen correspond to the ratio of PO_4, NO_3, and O_2 dissolved in the ocean (Redfield, 1958) and the Redfield ratios describe the relationship between the oxygen required to respire for the average marine organic matter composition (Redfield, 1934, 1958). In the deep water, the Redfield ratio of phosphorus to nitrogen is 1:16. Nitrate is typically the limiting nutrient for marine organic matter so the concentration of nitrate in the deep ocean determines the oxygen demand of respiration (Lenton and Watson, 2000). Redfield (1934, 1958) suggested that nitrogen fixing and denitrifying organisms may regulate the amount of nitrate in the ocean, via the Redfield ratio, and that nitrogen fixation can provide a negative feedback mechanism, where if phosphate increases in

the Redfield ratio, nitrogen fixing organisms will be given a selective advantage, which would increase nitrate in the ocean, and if phosphate decreases in the Redfield ratio, nitrogen fixation will be selected against and denitrification will reduce nitrate until the amount returns to the Redfield ratio. An increase in nitrate also increases new production, which leads to anoxia in the water-column. Denitrification occurs when oxygen concentration falls sufficiently low, but a decrease in nitrate will reduce anoxia and denitrification.

In the 1x CO_2 scenario (Fig. 14a), the Redfield ratio of NO_3 to PO_4 is simulated at 500 m, at the center of the equatorial Atlantic Ocean OMZ. Note that the lowest concentrations of NO_3 and PO_4 are simulated within the largest known OMZs. This is the opposite of the N:P predicted ratios for the Atlantic Ocean by Galbraith and Martiny (2015), which was based on observed PO_4 and NO_3 concentrations from the upper 30 m in the World Ocean Atlas, with the lowest N:P ratios in the Southern Ocean and the highest N:P ratios in between 50 °N and 50 °S. This discrepancy is likely due to the model being unable to resolve the ratio when values are too close to zero. A low N:P ratio has been observed in the high-latitude Southern Ocean, attributed to an abundance of phosphorus-rich molecules in cold phytoplankton which grow quickly. In contrast, oligotrophic regions tend toward a high N:P ratio, due to enhanced reliance on nitrate-rich proteins (Galbraith and Martiny, 2015). When the 4x CO_2 simulation is compared to the preindustrial control run (Figure 14b), the Redfield ratio skews towards NO_3, particularly in the North Atlantic Ocean. The higher Redfield ratio of N:P is more evident within the intermediate waters of the North Atlantic Ocean, likely due to an increase of POC flux from the increased NPP in this area. Conversely, there is a decrease in the Redfield Ratio of N:P within the equatorial Atlantic OMZ, which may be explained by an increase of denitrification with decreased DO. Overall, the ratio of nitrate to

phosphate concentrations in the Atlantic Ocean closely matched the Redfield ratio in the 4x CO_2 scenario, though there appears to be a slight skewing towards NO_3 (Fig. 16).

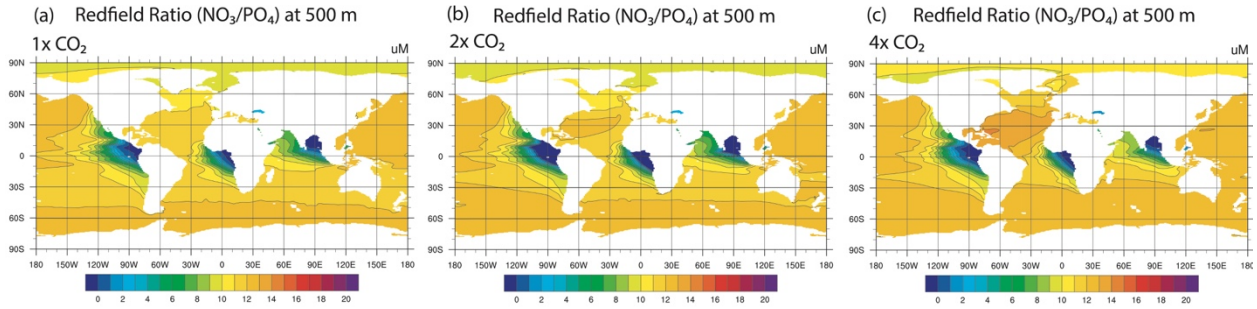

Figure 14. The Redfield Ratio (NO_3/PO_4) is simulated using CESM1.2 at 500 m for the 1x CO_2 experiment (a), the 2x CO_2 scenario (b), and for the 4x CO_2 scenario (c).

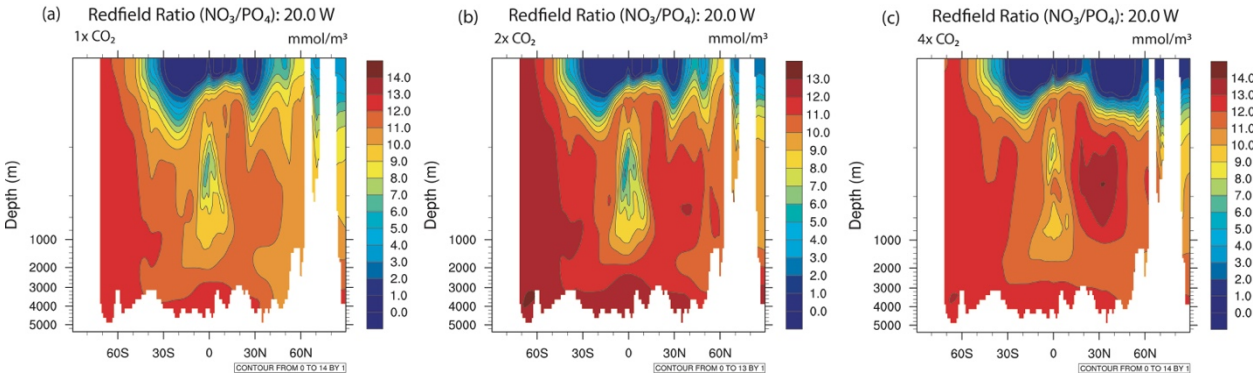

Figure 15. Cross-section of the Redfield ratio (NO_3/PO_4) in the Atlantic Ocean at 20 °W simulated with CESM1.2 for a 1x CO_2 experiment (a), the 2x CO_2 experiment (b), and the 4x CO_2 experiment.

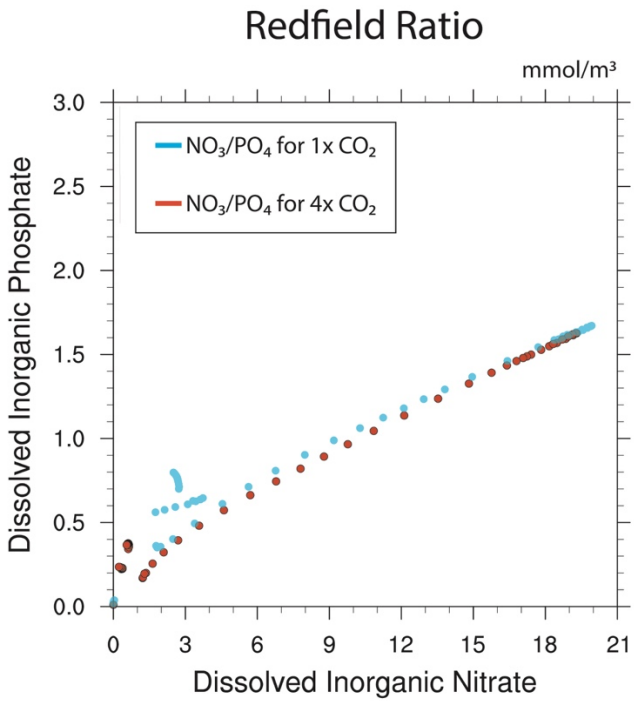

Figure 16. A scatter plot for the Redfield Ratio (NO_3/PO_4) simulated with CESM1.2 for 1x CO_2 (blue) and 4x CO_2 (red).

The Redfield ratio of NO_3 to PO_4 is fairly constant in marine organic matter, but can be altered with changes in the distributions of phytoplankton population that have different N:P ratios. Phytoplankton composition is known to have changed several times throughout Earth's history, the most recent being the evolution of diatoms 200 million years ago (Planavsky, 2014). For marine ecosystems, nitrogen fixation plays a critical role in the nitrogen cycle and changes in nitrogen fixing autotrophs, such as diazotrophs, may be significantly impacted. Redfield ratios were calculated from the CESM1.2.2 1x CO_2 run for large phytoplankton (16.9), small phytoplankton (16.9), diazotrophs (42.6), and small detritus (42.4). According to Justus von Liebig's law of minimum, the yield is proportional to the amount of the most limiting nutrient and based on these Redfield ratios, the diazotroph phytoplankton group limiting factor for growth is phosphorus. The diazotroph grow more slowly than other plankton types and depend

on an excess of iron and phosphorus over nitrogen (Berman-Frank et al., 2001), so they can be out competed if they are limited by iron or dissolved inorganic phosphorus. Diazotrophs can only co-exist with other phytoplankton species if they are nitrogen limited because of their low growth rate (Dutkiewicz et al., 2014). With an increase of stratification in the North Atlantic and a reduction in the AMOC, macronutrient supply to surface of the ocean and primary productivity at higher latitudes decrease, thus the competition of organism over these nutrients may rise. Diazotrophs' maximum growth rate is affected by an increase of temperature and they may have a more favorable environment with a lower macronutrient supply. This could explain the increase of diazotroph distribution in the North Atlantic Ocean at 40 °N (Fig. 17b) in the 4x CO_2 scenario, relative to the 1x CO_2 scenario (Fig. 17a). The change in higher diazotrophs and associated increased nitrogen fixation may contribute to higher Redfield ratio at this latitude increase and diazotroph-related POC flux.

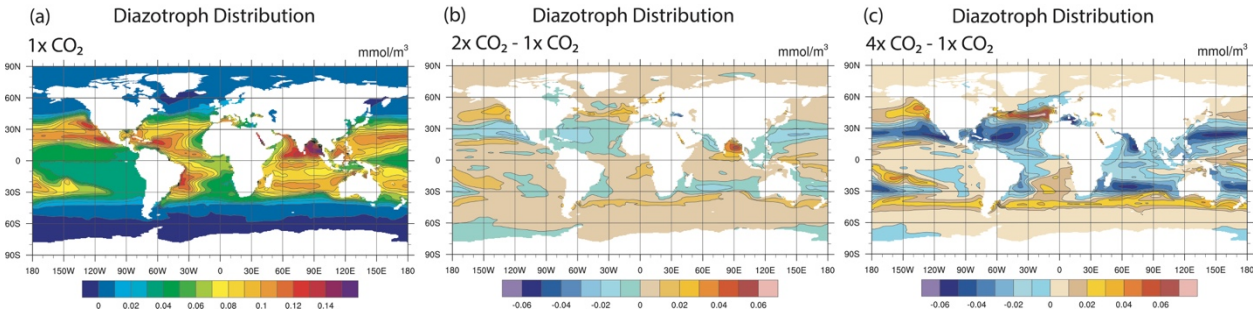

Figure 17. Surface level diazotroph distribution simulated using CESM1.2 for 1x CO_2 (a), for the difference between 2x CO_2 and 1x CO_2 (b), and for the difference between 4x CO_2 and 1x CO_2 (c).

Changes in DO concentration indicates physical and biological changes in the ocean (Stramma et al., 2008). Climate change simulations predict a decline in oxygenation throughout most parts of the ocean (Long et al., 2016). At the surface layer of the ocean, oxygen is saturated

because of the exchange with the overlying air. Wave entrainment and marine productivity can lead to a supersaturation. Increase in remineralization of POP in intermediate depth enhances the extent of the OMZ whereas ventilated North Atlantic Deep Water masses lead to DO increases in deeper levels below the OMZ (Brandt et al., 201). The concentration of oxygen in the ocean interior shows the balance between advection, diffusion and the biological-induced consumption (Frolicher et al., 2009). It has been predicted that anthropogenic climate change will lead to a vertical expansion of the oxygen minimum zone (OMZ) in the tropical northeast of the Atlantic Ocean (Stramma et al., 2012). In the eastern tropical Atlantic ocean, the OMZ exists between 100 and 900 m depth (Karstensen et al., 2008) and can be located in the shadow zone of the eastern boundary (Stramma et al., 2008). In the past five decades, a global oceanic oxygen loss has already been observed between 100 and 1000 m depth (Schmidtko et al., 2017).

In the 1x CO_2 scenario, the simulated extent of the OMZ in the Atlantic Ocean (Fig. 19) matches the observed OMZ of the World Ocean Atlas (NOAA, 2013) (Fig. 18), which occurs between 30 °N and 30 °S, however, the model OMZ is too exensive (Moore et al., 2013) along the equatorial region. In the 4x CO_2 experiment, DO concentrations are lower in the Southern Ocean, and in the North Atlantic Ocean compared to the 1x CO_2 scenario. DO concentrations decreases with depth, particularly centered around 1000 m. The shape of the OMZ is set by ocean circulation (Brandt et al., 2015), as well as increased stratification. A reduced AMOC strength and a reduction in the ventilation of the thermocline (Frolicher et al., 2009) could explain the vertical expansion of the OMZ in the 4x CO_2 scenario, compared to 1 x CO_2 scenario (Fig. 20), as well as the horizontal expansion towards the western basin of the Atlantic Ocean, where DO is decreasing (Fig. 19c). The oxygen reduction in the deep ocean of the North Atlantic Ocean with

CO_2 radiative forcing is linked to AMOC reduction and increase in biological oxygen utilization

Yamamoto et al., 2015).

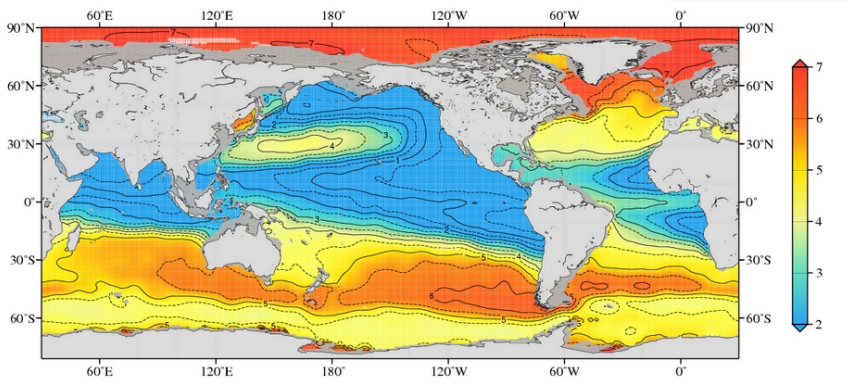

Figure 18. Annual oxygen [ml/l] at 550 m depth (one-degree grid) taken from the World Ocean Atlas 2018 (NOAA, 2018).

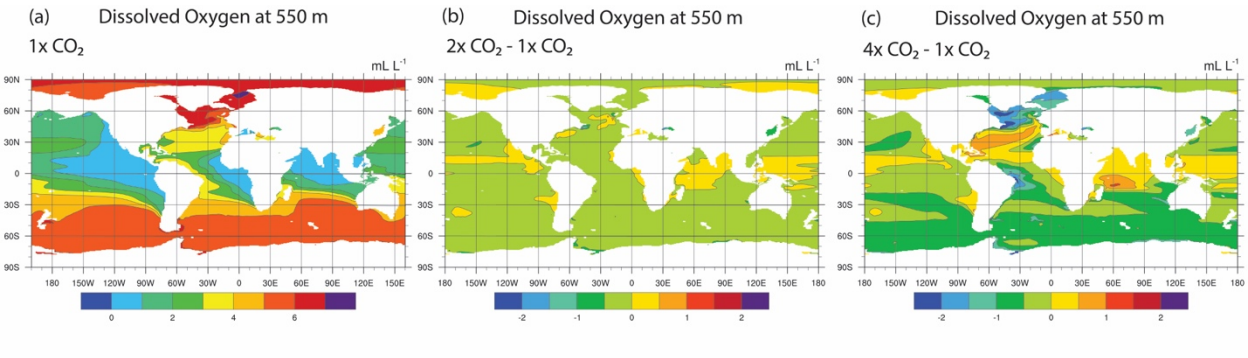

Figure 19. Dissolved oxygen concentration simulated at 550 m for 1x CO_2 experiment (a), differences between the 2x CO_2 experiment and 1x CO_2 experiment (b), and the differences between the 4x CO_2 experiment and 1x CO_2 experiment (c).

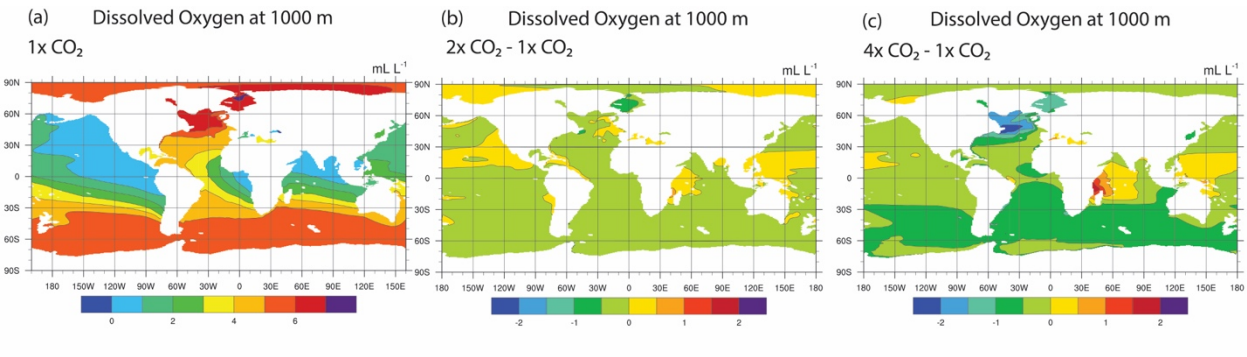

Figure 20. Dissolved oxygen concentration simulated at 1000 m for 1x CO_2 experiment (a), differences between the 2x CO_2 experiment and 1x CO_2 experiment (b), and the differences between the 4x CO_2 experiment and 1x CO_2 experiment (c).

A time series of global dissolved oxygen at 1000 m for 150 years is displayed (Fig 21). On average, dissolved oxygen decreased with increasing atmospheric pCO_2 and nearly equilibrates after 150 years of integration. There is a decline in oceanic dissolved oxygen concentration in intermediate depth with CO_2 radiative forcing (Stramma et al., 2008).

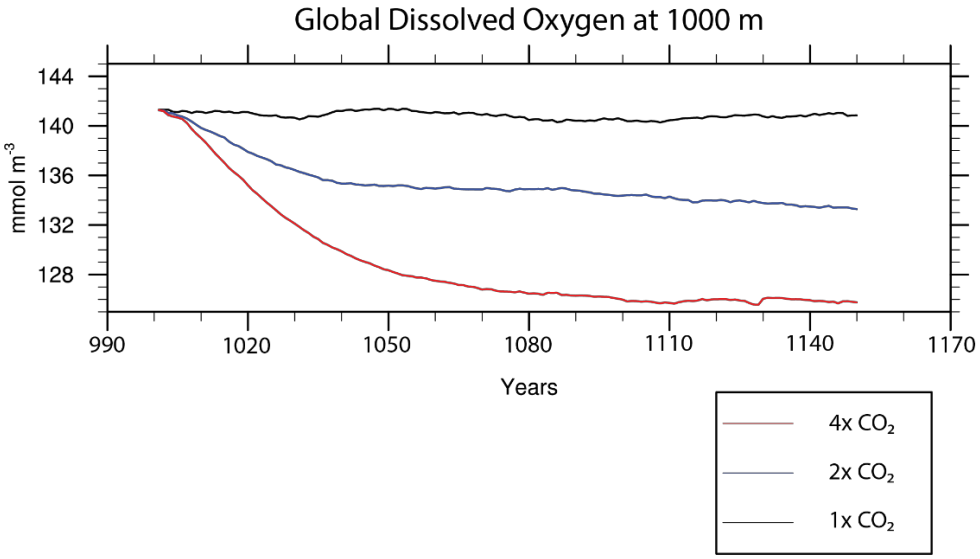

Figure 21. Global dissolved oxygen time series simulated at 1000 m for the 1x CO_2 scenario (black), 2x CO_2 scenario (blue), and 4x CO_2 scenario (red).

An oxygen minimum zone is simulated in the equatorial and tropical Atlantic Ocean at 10 °N in the 1x CO_2 simulation (Fig. 22). With increased levels of atmospheric pCO_2, a slight increase of DO is observed within the euphotic zone of the North Atlantic Ocean and the upper 1000 m of this oxygen minimum zone, as predicted by other climate models (Strama et al., 2008). However, dissolved oxygen levels are decreasing at, and below, 1000 m which could be linked to enhanced stratification. The decreased dissolved oxygen concentration in the deep ocean may be attributed to reduced ventilation, which is caused by the reduced AMOC, and therefore, the

oxygen is residing longer in the deep ocean, giving it more time to be consumed by biological activity (Yamamoto et al., 2015).

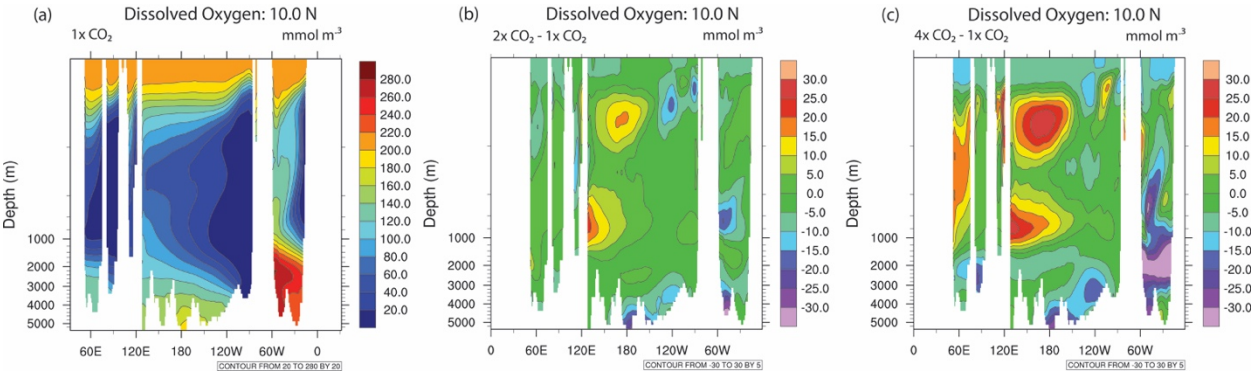

Figure 22. Cross-section of dissolved oxygen concentration in the Atlantic Ocean at 10 ˚N simulated with CESM1.2 for 1x CO_2 experiment (a), differences between the 2x CO_2 experiment and 1x CO_2 experiment (b), and differences between the 4x CO_2 experiment and 1x CO_2 experiment (c).

Oxygen production occurs in the euphotic zone by photosynthesis and, along 20 ˚W, primarily in the tropical region, Southern Ocean, and in the North Atlantic Ocean (Fig. 23). A small decrease of oxygen production occurs along the equator and North Atlantic Ocean, in the 2x CO_2 scenario, and decreases further in the North Atlantic for the 4x CO_2 scenario. Enhanced upper-ocean stratification in the equatorial and tropical Atlantic Ocean could lead to a decrease of Ekman-induced upwelling in nutrients to the surface, which would result in a decline of net primary production (Beaty et al., 2017, Schmidtko et al., 2017). The decrease in oxygen production in the North Atlantic Ocean could be due to the slowdown of the AMOC, which changes the water mass distribution (Brandt et al., 2015).

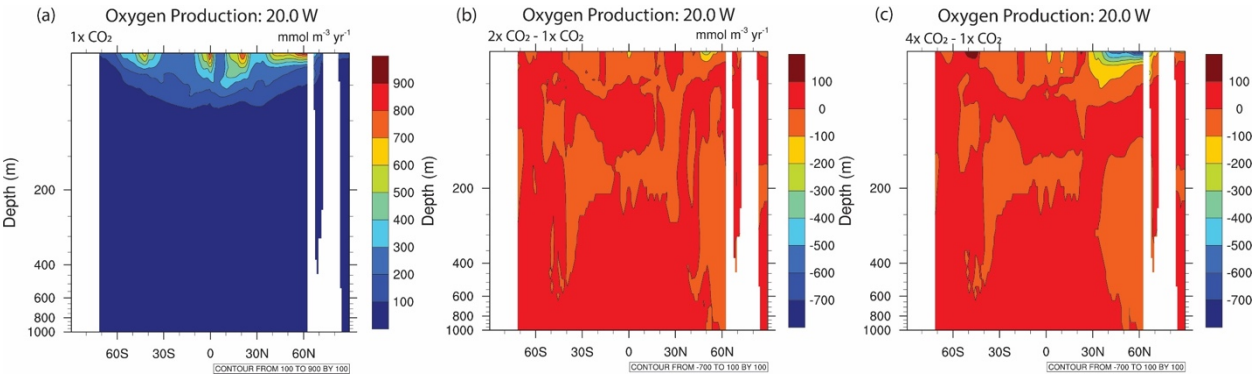

Figure 23. Cross-section of production of dissolved oxygen concentration in the Atlantic Ocean at 20 ˚W simulated with CESM1.2 for 1x CO_2 experiment (a), differences between the 2x CO_2 experiment and 1x CO_2 experiment (b), and differences between the 4x CO_2 experiment and 1x CO_2 experiment (c).

DO is consumed by remineralization of sinking organic matter, related to marine life metabolism and elementary chemical reactions. DO consumption can be enhanced from elevated primary production. This would result in increased respiration when particles sink in the water column (Brandt et al., 2015). Remineralization decreases with depth and therefore it is unlikely that there will be large changes in consumption below 1000 m (Schmidtko et al., 2017). Areas of increased biological activity from primary production occur along the equatorial Atlantic Ocean, within the euphotic zone (Fig. 24). When atmospheric pCO_2 are doubled and quadrupled, DO consumption increases at most depths except for the upper North Atlantic Ocean. Enhanced remineralization and biological productivity in an area with a shallow mixed layer could explain this decrease (Karstensen et al., 2008). There is, however an increase of DO consumption near 30 ˚N, where net primary production appears to increase.

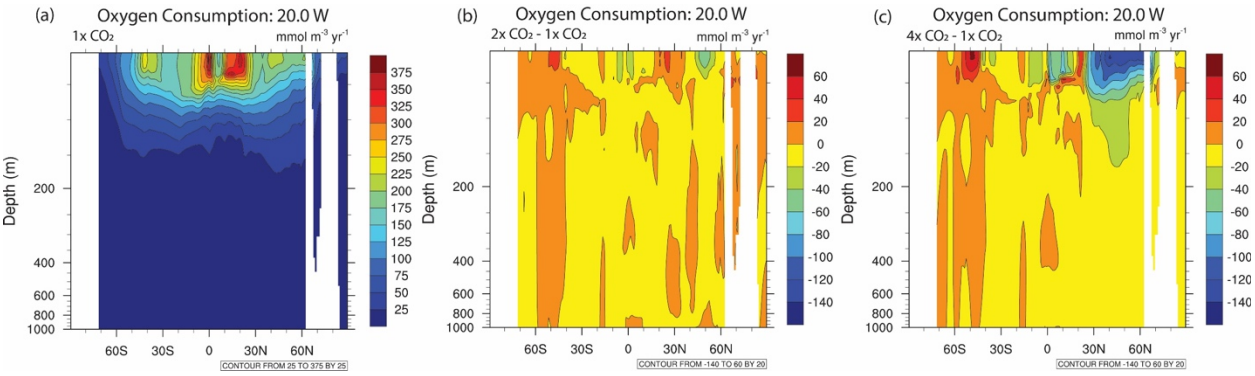

Figure 24. Cross-section of consumption of dissolved oxygen concentration in the Atlantic Ocean at 20 ˚W simulated with CESM1.2 for 1x CO_2 experiment (a), differences between the 2x CO_2 experiment and 1x CO_2 experiment (b), and differences between the 4x CO_2 experiment and 1x CO_2 experiment (c).

DO saturation (O_2sat) is calculated from in situ temperature and salinity and it represents DO concentration at equilibrium (Cabre et al, 2016). Due to an increase of ocean temperatures from global warming, DO saturation is expected to decline (Schmidtko et al., 2017). In the 1x CO_2 scenario (Fig. 25), oxygen saturation is highest near the poles in the Atlantic Ocean and lowest in the tropical latitudes. With increasing temperatures, oxygen saturation decreases. This is most evident in the Southern Ocean, where temperatures are predicted to increase, and within the OMZ of the equatorial Atlantic Ocean. DO saturation levels increase in the 4x CO_2 senario relative to the 1x CO_2 senario where temperatures decrease.

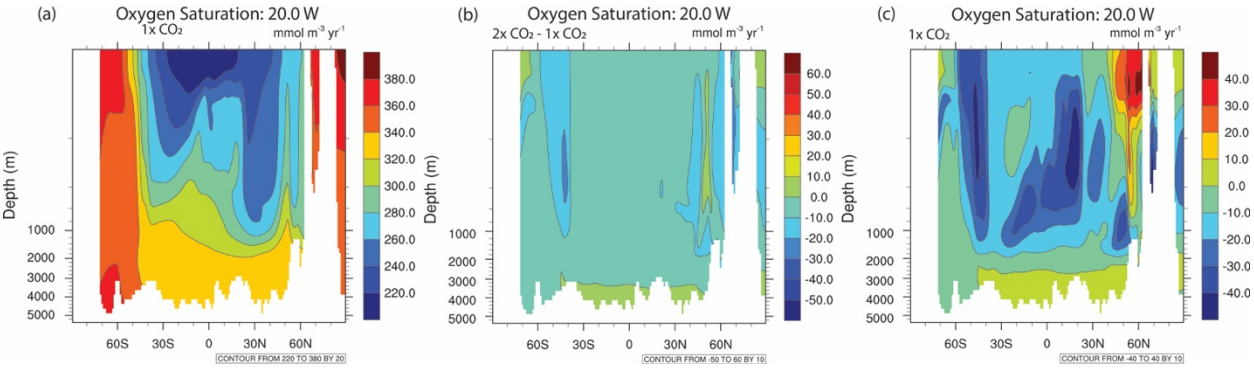

Figure 25. Cross-section of apparent oxygen saturation in the Atlantic Ocean at 20 ˚W simulated with CESM1.2 for 1x CO_2 experiment (a), differences between the 2x CO_2 experiment and 1x CO_2 experiment (b), and differences between the 4x CO_2 experiment and 1x CO_2 experiment (c).

The AOU distribution (Fig. 26) represents a reasonable approximation of the accumulated biologic-induced oxygen consumption since the parcel of water left the surface (Cabre et al., 2015). The subpolar North Atlantic (SPNA), lower solubility and an increase in AOU is predicted to result in a decline in oceanic oxygen (Tjiputra et al., 2018). AOU is highest within the OMZ of the tropical Atlantic Ocean for the 1x CO_2 (Fig. 26), but it decreases within this region with an increase of atmospheric pCO_2. Reduced ocean ventilation contributes to an increase in the extent of the OMZ and in AOU (Karstensen et al., 2008). The increase of AOU in the Southern Ocean with CO2 radiative forcing can be attributed to increased remineralization from increased biological consumption.

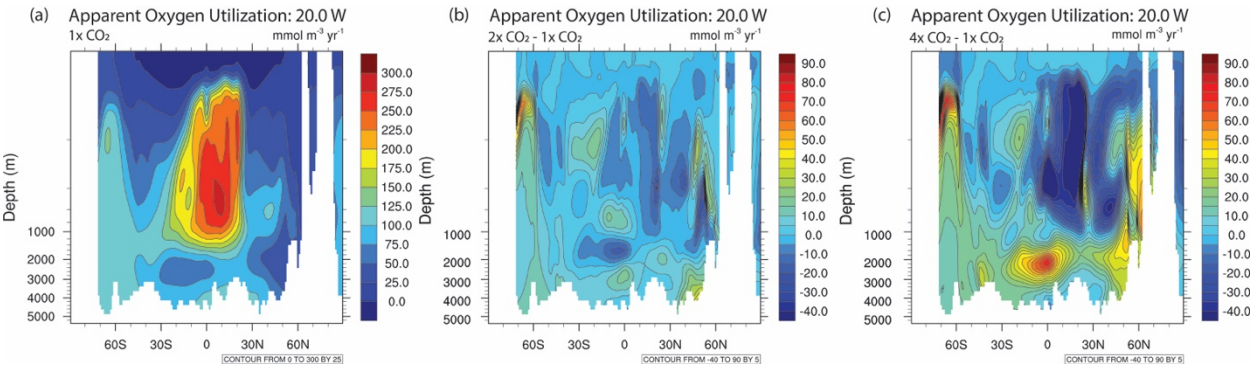

Figure 26. Apparent Oxygen Utilization (AOU) simulated in the Atlantic Ocean, along 20 °W, for 1x CO_2 (a) and compared to 2x CO_2 (b) and 4x CO_2 (c).

Chapter Five: Discussion

Under global warming scenarios, increased stratification, a slow-down of the AMOC, and a reduction of ventilation of the thermocline are responsible for reducing oxygen concentration and nutrient-rich waters being upwelled. An increase of idealized age and residence time of water in the deep ocean is also observed in climate change scenarios. Oxygen solubility and AOU gas exchange drives the decline of oxygen in the thermocline of the Atlantic Ocean (Frolicher et al., 2009). Reduced ventilation affects the extend of the OMZ, but the advection of well-ventilated water from the South Atlantic Ocean into the OMZ region compensates the expansion of the OMZ (Karstensen et al., 2008). The slowing down of the AMOC may also be responsible to decreased DO concentration. Moreover, reduction of summer ice and associated increased biological activity with increase in insolation and sea surface temperatures could alter DO concentration (Schmidtko et al., 2017).

The zonal mean oxygen concentration is decreasing at 1000 m, thus contributing to a vertical expansion of the OMZ, even though the zonal mean of oxygen is increasing between 200 and 1000 m in the Atlantic Ocean (Stramma et al., 2008). A horizontal expansion towards the western basin of the Atlantic OMZ also occurs as CO_2 radiative forcing increases. It is important to note that there may be a negative model-data bias of DO concentration in the tropics in climate models because CESM tends to underestimate the amplitude of interannual variability in oxygen (Long et al., 2016). Vertical expansion of the OMZ is predicted for the tropical northeast Atlantic Ocean, and this could have significantly negative impacts on available habitats for

tropical pelagic fishes and fishing (Stramma et al., 2012). Declining oxygen levels, and an expansion of the OMZ, also affect carbon and nitrogen cycles, which negatively affects marine ecosystems and fisheries (Stramma et al., 2010).

There is a need to continue the model integration for a longer period of time, because of the long adjustment time of circulation and tracer in the deep-sea. In other model studies, oxygen concentration has been observed to decrease for the first 500 years, but then recovers despite a weakened AMOC and decrease in surface oxygen. This is possibly due to enhanced ventilation in the Southern Ocean (Yamamoto et al., 2015).

Chapter Six: Conclusion

In conclusion, an increase in temperature due to CO_2-radiative forcing produces a global decline of dissolved oxygen concentration and saturation levels and thus a vertical downward and horizontal westward expansion in the Atlantic OMZ. This decrease in DO concentration at intermediate depth in the tropical eastern Atlantic Ocean is driven by enhanced stratification and the slow-down of the AMOC. In the 4x CO_2 scenario, reduced Ekman-induced upwelling and a more stratified ocean are resulting in a decrease of NPP. In the future, this simulation needs to be extended so that temporal adjustment of OMZs in the Pacific and Indian Ocean may be achieved.

References

Archer, D. 2003. Biological fluxes in the ocean and atmospheric pCO2. *Treatise on Geochemistry,* 6, 275-291. doi: 10.1029/1999GB001216

Bakun, A., Black, B. A., Bograd, S. J., Garcia-Reyes, M., Miller, A. J., Rykaczewski, R. R., Sydeman, W. J. 2015. Anticipated effects of climate change on coastal upwelling ecosystems, *Curr. Clim. Change Rep.*, 1,85-93. doi: 10.1007/s40641-015-0008-4

Beaty, T., Heinze, C., Hughlett, T., Winguth, A. M. E. 2017.Response of export production and dissolved oxygen concentrations in oxygen concentrations in oxygen minimum zones to pCO_2 and temperature stabilization scenarios in the biogeochemical model HAMOCC 2.0. *Biogeosciences*, 14, 781-797.doi: 10.5194/bg-14-781-2017

Berman-Frank, I., Lundgren, P., Chen, Y. B., Kupper, H., Kolber, Z., Bergman, B., Falkowski, P. 2001. Segregation of nitrogen fixation and oxygenic photosynthesis in the marine Cyanobacterium Trichodesmium. Science, 294(5546), 1534-1537. doi: 10.1126/science.1064082

Boyd, P.W., Sundby, S., Portner, H.O. 2014. Cross-chapter box on net primary production. In: climate change 2014: Impacts, cdaptation and vulnerability. *Part A: Global and Sectoral Aspects. Contribution of Working Group II to the Fifth Assessment Report of the Intergovernmental Panel on Climate Change*,133-136.

Brandt, P., Bange, H. W., Banyte, D., Dengler, M., Didwischus, S. H., Fischer, T., Greatbatch, R. J., Hahn, T. K., Karstensen, J., Kortzinger, A., Krahmann, G., Schmidtko, S., Stramma, L., Tanhua, T., Visbeck, M. 2015. On the role of circulation and mixing of oxygen minimum zones with a focus on the eastern tropical North Atlantic. *Biogeosciences*,12, 489-512. doi: 10.5194/bg-12-489-2015

Bryan, F. O., Danabsoglu, G. Nakashiki, N., Yoshida, Y., Kim, D. H., Tsutsui, J., Doney, S. C. 2006. Response of the North Atlantic thermohaline circulation and ventilation to Increasing carbon dioxide in CCSM3. *Journal of Climate*, 19, 2382-2397. doi:10.1175/JCL13757.1

Cabre, A., Marinov, I., Bernadello, R., Bianchi, D. 2015. Oxygen minimum zones in the tropical Pacific across CMIP5 models: mean state differences and climate change trends. *Biogeosciences*,12, 5429-5454. doi: 10.5194/bg-12-5429-2015

Caesar, L., Rahmstorf, S., Robinson, A., Feulner, G., Saba, V. 2018. Observed fingerprint of a weakening Atlantic Ocean overturning circulation. *Nature*, 556, 191-196. doi:10.1038_s41586-018-0006-5.ris

Cropper, T., Hanna, E., Bigg, G. 2014. Spatial and temporal seasonal trends in coastal upwelling off Northwest Africa, 1981-2012. *Deep-Sea Research I*, 86, 94-111. doi: 10.1016/j.dsr.2014.01.007

Cox, P. M., Betts, R. A., Jones, C. D., Spall, S. A., Totterdell, I. J. 2000. Acceleration of global warming due to carbon-cycle feedbacks in a coupled climate model. *Nature*, 408, 184-187. doi: 10.1038/35041539

de Boyer Montegut, C., Madee, G., Fischer, A. S., Lazar, A., Iudicone, D. 2004. Mixed layer depth over the global ocean: An examination of profile data and a profile-based climatology. *Journal of Geophysical Research*, 109, C12003. doi: 10.1029/2004jc002378

Deutsch, C., Brix, H., Ito, T., Frenzel, H., Thompson, L. 2011. Climate-forced variability

of ocean hypoxia. *Science*, 333(6040), 336-338. doi: 10.1126/science.1202422
Dufresney, J. L., Friedlingstein, P., Berthelog, M., Bopp, L., Ciais, P., Fairhead, L., Treut, H. L., Monfray, P. 2002. On the magnitude of positive feedback between future climate change and the carbon cycle. *Geophys. Res. Lett*., 29, 1405. doi:10.1029/2001GL013777
Dutkiewicz, S., Ward, B. A., Scott, J. R., Follows, M. J. 2014. Understanding predicted shifts in diazotroph biogeography using resource competition theory. *Biogeosciences*, 11, 5445-5461. doi: 10.5194/bg-11-5445-2014
England, M. H. 1995. The age of water and ventilation timescales in a global ocean model. *Journal of Physical Oceanography*, 25, 2756-2777. doi: 10.1175/1520-00485
Erwin, D. H. 2006. *Extinction: How life on earth nearly ended 250 million years ago*, Princeton Univ. Press, Princeton, N. J.
Falkowski, P. G. 1997. Evolution of the nitrogen cycle and its influence on the biological sequestration of CO_2 in the ocean. *Nature*, 387, 272-275. doi: 10.138_38727
Frolicher, T.L., Joos, F., Plattner, G. K., Steinacher, M., Doney. 2009. Natural variability and anthropogenic trends in oceanic oxygen in a coupled carbon cycle-climate model ensemble. *Global Biogeochemical Cycles*, 23, GB1003. doi: 10.1029/2008gb003316
Galbraith, E. D., Martiny, A. C. 2015. A simple nutrient-dependence mechanism for predicting the stoichiometry of marine ecosystems, *PNAS*, 112(27), 8199-8204. doi: 10.1073/pnas.1423917112
Geider, R. J., MacIntyre, H. L., Kana, T. M. 1998. A dynamic regulatory model of phytoplankton acclimation to light, nutrients, and temperature. *Limnology and Oceanography*, 43, 679-694. doi: 10.4319/lo.1998.43.4.0679
Gent, P. R., Danabasoglu, G., Doner, L. J., Holland, M. M., Hunke, E. C., Jayne, S. R., Lawrence, D. M., Neal, R. B., Rasch, P. J., Vertenstein, M., Worley, P. H., Yang, Z, Zhang, M. 2011. The Community Climate System Model Version 4. *Journal of Climate*. 24(19), 4973-4991. doi: 10.1175/2011jcl14083.1
Gnanadesikan, A., Russell, J. L., Zeng, F. 2007. How does ocean ventilation change under global warming? *Ocean Sci*. 3(4), 43-53. doi: 10.5194/osd-3-805-2006
Gruber, N. (2008). Marine nitrogen cycle: overview and challenges. *Nitrogen in the Marine Environment.* Douglas GC, Deborah AB, Margaret RM, Edward JC. Nitrogen in the marine environment (2nd edition): Academic Press 1-50.
Gruber, N. 2011. Warming up, turning sour, losing breath: ocean biogeochemistry under global change. *Phil. Trans.R. Soc. A*, 369, p. 1980-1996. doi: 10.1098/rsta.2011.0003
Hsieh, W. W., Boer, G. J. 1992. Global climate change and ocean upwelling. *Fisheries Oceanography*, 1(4), 333-338. doi: 10.1111/j.1365-2419.1992.tb00005.x
Hurrell, J. W., Holland, M. M., Gent, P. R., Ghan, S. Kay, J. E., Kushner, P. J., Lamarque, J. F., Large, W. G., Lawrence, D., Lindsay, K., Lipscomb, W. H., Long, M. C. Mahowald, N., Marsh, D. R., Neale, R. B. Rasch, P., Vavrus, S., Vertenstein, M., Bader, D., Collins, W. D., Hack, J. J., Kiehl, J., Marshall, S. 2013. The community Earth system model: a framework for collaborative research. *Bams*. 1339-1360. doi: 10.1175/bams-d-12.00121.1
IPCC, 2013: Climate change 2013: the physical science basis. contribution of working group I to the fifth assessment report of the intergovernmental panel on climate change [Stocker, T.F., D. Qin, G.-K. Plattner, M. Tignor, S.K. Allen, J. Boschung, A. Nauels, Y. Xia, V. Bex and P.M. Midgley (eds.)]. Cambridge University Press, Cambridge, United Kingdom and New York, NY, USA, 1535 pp, doi:10.1017/CBO9781107415324

Karstensen, J., Stramma, L., Visbeck, M. 2008. Oxygen minimum zones in the eastern tropical Atlantic and Pacific oceans. *Progress in Oceanography*. 77(4), 331-350. doi: 10.1016/j-pocean.2007.05.009

Karstensen, J., Fielder, B., Schütte, F., Brandt, P., Kortzinger, A., Fischer, G., Zantopp, R., Hahn, J., Visbeck, M., Wallace, D. 2015. Open ocean dead zones in the tropical North Atlantic Ocean, *Biogeosciences*, 12, 2597-2605. doi: 10.5194/bg-12-2597-2015

Keeling, C. D., Piper, S. C., Bacastow, R. B., Wahlen, M., Whorf, T. P., Heimann, M., Meijer, H. A. Exchanges of atmospheric CO_2 and $^{13}CO_2$ with the terrestrial biosphere and oceans from 1978 to 2000. I. Global aspects, SIO Reference Series, No. 01-06, Scripps Institution of Oceanography, San Diego, 88 pages, 2001

Keeling, R. F., Garcia, H. E. 2002. The change in oceanic O_2 inventory associated with recent global warming. *Proc. Natl. Acad. Sci. U.S.A*., 99(12), 7848-7853. doi:10.1073/pnas.122154899

Knoll, A. H., Carroll, S. B. 1999. Early animal evolution: Emerging views from comparative biology and geology. *Science*, 284, 2129-2137, doi:10.1126/science.284.5423.2129.

Lauderdale, J. M., Naveira Garaboto, A. C., Oliver, K. I. C., Follows, M. J., Williams, R. G. 2013. Wind-driven changes in Southern Ocean residual circulation, ocean carbon reservoirs and atmospheric CO_2. *Climate Dynamics*, 41(7-8), 2145-2164. doi: 10.1007/s00382-012-1650-3

Lindsay, K., Bonan, G. B., Doney, S. C., Hoffman, F. M. Lawrence, D. M., Long, M. C., Mahowald, N. M., Moore, J. K., Randerson, J. T., Thornton, P. E. 2014. Preindustrial-control and cwentieth-century carbon cycle cxperiments with the Earth cystem model CESM1(BGC). *Journal of Climate*, 27, 8981-9005, doi:10.1175/JCLI-D_12-00565.1

Lenton, T. M. Watson, A. J. 2015. Redfield revisited 1. Regulation of nitrate, phosphate, and oxygen in the ocean. *Global Biogeochemical Cycles*, 14 (1), 225-248. doi: 10.1029/1999GB900065

Long, M. C., Deutsch, C., Ito, T. 2016. Finding forced trends in oceanic oxygen. *Global Biochemical Cycles*, 30, 381-397. doi:10.1002/2015GB005310

Manabe, S., Stouffer, R. J., Spelman, M. J., Bryan, K. 1991. Transient responses of a coupled Ocean-atmosphere model to gradual changes of atmospheric CO_2. Part I: annual mean response, *Journal of Climate*, 4, 785-818. doi: 10.1175/1520-0442

Manabe, S., Stouffer, R. J. 1993. Century-scale effects of increased atmospheric CO_2 on the ocean-atmosphere system. *Nature*, 364,215-218. doi: 10.1038/364215a0

Matear, R. J. 2003. Long-term changes in dissolved oxygen concentrations in the ocean caused by protracted global warming. *Global Biogeochemical Cycles*, 17(4), 1125. doi: 10.1029/2002gb001997

Moore, J. K., Doney, S. C., Glover, D. M., Fung, I. Y. 2002. An intermediate complexity marine ecosystem model for the global domain. *Deep-Sea Res. II*, 49,403-462

Moore, J. K., Doney, S. C., Lindsay, K. 2004. Upper ocean ecosystem dynamics and iron cycling in the global three-dimensional model. *Global Biogeochem. Cycles*, 18, GB4028, doi:10.1029/2004GB002220

Moore, J. K., Lindsay, K., Doney, S. C., Long, M. C., Misumi, K. 2013.Marine ecosystem dynamics and biogeochemical cycling in the community Earth system model [CESM1(BGC)]: Comparison of the 1990s with the 2090s under the RCP4.5 and RCP8.5 scenarios. *Journal of Climate*, 26(23), 9291-9312. doi: 10.1175/jcli-d-12-00566.1

National Oceanic and Atmospheric Administration. 2018.

https://www.nodc.noaa.gov/cgi-bin/OC5/woa18f/woa18oxnuf.pl
National Oceanic and Atmospheric Administration. 2019. (https://www.esrl.noaa.gov/gmd/ccgg/trends/)
Pena, M. A., Katseve, S., Oguz, T., Gilbert, D. 2010. Modeling dissolved oxygen dynamics and hypoxia. *Biogeosciences,* 7, p. 933-957. doi: 10.5194/bg-7-933-2010
Climate and atmospheric history of the past 420,000 years from the Vostok ice core, Antarctica. *Nature*, 399(6735), 429-436. doi: 10.1038/20859
Planavsky, N. J. 2014. The elements of marine life. *Nature Geoscience*, 7, 855-856. doi: 10.1038/ngeo2307
Praetorius, S. 2018. North Atlantic circulation slows down. *Nature*. 556, 180-181.
Rahmstorf, S., Willebrand, J. 1995. The role of temperature feedback in stabilizing the thermohaline circulation. *J. Phys. Oceanogr.*, 25, 787-805. doi:10.1175/1520-0485(1995)025<0787:TROTFI>2.0.CO;2
Randelhoff, A., Sundfjord, A. 2018. Short commentary on marine productivity at Arctic shelf breaks: upwelling, advection and vertical mixing. *Ocean Sci. Discuss*. 14, 293-300. doi: 10.5194/os-2017-68
Redfield, A. C. 1934. On the proportions of organic derivatives in sea water and their relation to the composition of plankton: *University Press of Liverpool*, 176-192.
Redfield, A. C. 1958.The biological control of chemical factors in the environment, *Am. Sci*, 46 (3), 205-221.
Ruiz-Barradas, A., Chafik, L., Nigam, S., Hakkinen, S. 2018. Recent subsurface North Atlantic cooling trend in context of Atlantic decadal-to-multidecadal variability. *Tellus A*, 70, 1481688. doi:10.1080/16000870.2018.1481688
Sarmiento, J. L., Slater, R., Barber, R., Bopp, L., Doney, S. C., Hirst, A. C., Kleypass, J., Matear, R., Mikolajewicz, U., Monfray, P., Soldatov, V., Spall, S. A., Stouffer, R. 2004. Response of ocean ecosystems to climate warming, *Global Biogeochemical Cycles*, 18, GB3003. doi: 10.1029/2003gb002134
Schmidtko, S., Stramma, L., Visbeck, M. 2017. Decline in global oceanic oxygen content during the past five decades. *Nature*. 542, 335-339. doi: 10.1038/nature21399
Smith, S. L., Yamanaka, Y., Pahlow, M., Oschlies, A. 2009. Optimal uptake kinetics: physiological acclimation explains the pattern of nitrate uptake by phytoplankton in the ocean. *Mar. Ecol. Prog. Ser*. 384, 1-13. doi: 10.3354/meps08022
Somavilla, R., Gonzalez-Pola, C., Fernandez-Diaz, J. 2017. The warmer the ocean surface, the shallower the mixed layer. How much of this is true? *J. Geophy. Res.Oceans*, 122, p. 7698-7716. doi: 10.1002/2017jc013125
Stanley, R. H. R., Doney, S. C., Jenkins, W. J., Lott, D. E. III. 2012. Apparent oxygen utilization rates calculated from tritium and helium-3 profiles at the Bermuda Atlantic time-series study site. *Biogeosciences*, 9, 1969-1983. doi:10.5194/bg-9-1969-2012
Stommel, H. M, Aarons, A. B. 1960. On the abyssal circulation of the world ocean – I. Stationary planetary flow patterns on a sphere. *Deep-Sea Res*, 6, 140-154
Stramma, L., Prince, E. D., Schmidtko, S., Luo, J., Hoolihan, J. P., Visbeck, M., Wallace, D. W. R., Brandt, P., Kortzinger, A. 2001. Expansion of oxygen minimum zones may reduce available habitat for tropical pelagic fishes. *Nature Climate Change*, 2, 33-37. doi: 10.1038/nclimate1304
Stramma, L., Johnson, G. C., Sprintall, J., Mohrholz, V. 2008. Expanding oxygen-minimum zones in the tropical oceans. *Science*, 320(5876), 655-658. doi:

10.1126/science.1153847
Stramma, L., Brandt, P., Schafstall, J., Schott, F., Fischer, J., Kortzinger, A. 2008. Oxygen minimum zone in the North Atlantic south and east of the Cape Verde islands. *Journal of Geophysical Research*, 113, C04014. doi: 10.1029/2007jc004369
Stramma, L., Schmidtko, S., Levin, L. A., Johnson, G. C. 2010. Ocean oxygen minima expansions and their biological impacts. *Deep-Sea Research I*., 57(4), 587-595. doi:10.1016/j.dsr.2010.01.005
Stramma, L., Prince, E. D., Schmidtko, S., Luo, J., Hoolihan, J. P., Visbeck, M., Wallace, D. W. R., Brandt, P., Kortzinger, A. 2012. Expansion of oxygen minimum zones may reduce available habitat for tropical pelagic fishes. Nature Climate Change, 2, 33-37. doi: 10.1038/nclimate1304
Thiele, G., Sarmiento, J. L. 1990. Trace dating and ocean ventilation. *JGR Oceans*, 95(C6), 9377-9391. doi: 10.1029/JC095iC06p09377
Tjiputra, J. F., Goris, N., Lauvset, S. K., Heinze, C., Olsen, A., Schwinger, J., Steinfeldt, R. 2018. Mechanisms and early detections of multidecadel oxygen changes in the interior subpolar North Atlantic. *Geophysical Research Letters*, 45. 4218-4229. doi: 10.1029/2018gl077096
Velez-Belchi, P. and Tintore, J. 2000. Vertical velocities at an ocean front. *Sci. Mar.*, 65, 291-300. doi: 10.3989/scimar.3001.65s1291
Volk, T., Hoffert, M. I. (1985) Ocean carbon pumps: analysis of relative strengths and efficiencies in ocean-driven atmospheric CO_2 changes. IN E. T. Sundquist & W. S. Broeker (Eds.), The carbon cycle and atmospheric CO_2: natural variations Archean to present. Chapman conference papers, 1984, p. 99-110. *American Geophysical Union*; Geophysical Monograph 32
Wanninkhof, R. 1992. Relationship between wind speed and gas exchange over the ocean. *Journal of Geophysical Research: Oceans*, 97, C5. doi:10.1029/92JC00188
Watson, A. J., Lenton, T. M., Mills, B. J. 2017. Ocean deoxygenation, the global phosphorus cycle and the possibility of human-caused large-scale ocean anoxia. *Phil. Trans. R. Soc. A*, 375, 20160318. doi:10.1098/rsta.2016.0318
Weiss, R.F. 1974. Carbon dioxide in water and seawater: the solubility of non-ideal gas. *Marine Chemistry,* 2(3), 203-215. doi: 10.1016/0304-4203(74)90015-2
Yamamoto, A., Abe-Ouchi, A., Shigemitsu, M., Oka, A., Takahashi, K., Ohgaito, R., Yamanaka, Y. 2015. Global deep ocean oxygenation by enhanced ventilation in the Southern Ocean under long-term global warming. *Global Biogeochem. Cycles*, 29, 1801-1815. doi: 10.1002/2015gb005181